[redacted]

ORNL
MASTER COPY

15

ORNL-3456
C-44b – Nuclear Technology – Chemistry and Chemical Engineering
M-3679 (31st ed.)

AEC RESEARCH AND DEVELOPMENT REPORT

RECOVERY OF URANIUM FROM GRAPHITE FUELS BY OXIDATION AND FLUORINATION

II. USE OF A MATHEMATICAL ANALYSIS OF THE OXIDATION PROCESS IN FIXED BEDS TO PREDICT PROCESS CONDITIONS

(Title Unclassified)

C. D. Scott

DECLASSIFIED By Authority Of: AEC (J. H. Kahn) 6-2-71
M. Shirley
For: N. T. Gray, Supervisor
Laboratory Records Dept.
ORNL

SPECIAL REVIEW FINAL DETERMINATION
CLASS. U AUTH.
REVIEWERS/VERIFIERS CLASS. DATE
(1) [illegible] U 7/2/80
(2) [illegible] U 6/13/80

OAK RIDGE NATIONAL LABORATORY
operated by
UNION CARBIDE CORPORATION
for the
U.S. ATOMIC ENERGY COMMISSION

[redacted]

[redacted]

[redacted]

LEGAL NOTICE

This report was prepared as an account of Government sponsored work. Neither the United States, nor the Commission, nor any person acting on behalf of the Commission:

A. Makes any warranty or representation, expressed or implied, with respect to the accuracy, completeness, or usefulness of the information contained in this report, or that the use of any information, apparatus, method, or process disclosed in this report may not infringe privately owned rights; or

B. Assumes any liabilities with respect to the use of, or for damages resulting from the use of any information, apparatus, method, or process disclosed in this report.

As used in the above, "person acting on behalf of the Commission" includes any employee or contractor of the Commission, or employee of such contractor, to the extent that such employee or contractor of the Commission, or employee of such contractor prepares, disseminates, or provides access to, any information pursuant to his employment or contract with the Commission, or his employment with such contractor.

[redacted]

ORNL-3456

Contract No. W-7405-eng-26

CHEMICAL TECHNOLOGY DIVISION

Unit Operations Section

RECOVERY OF URANIUM FROM GRAPHITE FUELS BY OXIDATION AND FLUORINATION

II. USE OF A MATHEMATICAL ANALYSIS OF THE OXIDATION PROCESS IN FIXED BEDS TO PREDICT PROCESS CONDITIONS

C. D. Scott

DATE ISSUED

JAN 22 1964

OAK RIDGE NATIONAL LABORATORY
Oak Ridge, Tennessee
operated by
UNION CARBIDE CORPORATION
for the
U.S. ATOMIC ENERGY COMMISSION

[redacted]

[redacted]

[redacted]

[redacted]

[redacted]

[redacted]

CONTENTS

		Page
	Abstract	1
1.	Introduction	2
2.	Process Flowsheet	3
3.	Reaction Kinetics	3
	3.1 Chemical Reactions	5
	3.2 Graphite Oxidation	6
	3.2.1 First-Order Kinetics	6
	3.2.2 External Mass Transport	7
	3.2.3 Internal Mass Transport	9
	3.3 Carbon Monoxide Oxidation	11
4.	Physical Properties	12
	4.1 Gas Properties	12
	4.2 Graphite-Uranium Fuel Properties	14
5.	Heat Generation and Heat Transfer	14
	5.1 Heat Generation	15
	5.2 Heat Transfer Mechanisms	15
	5.2.1 Radiative Heat Transfer	15
	5.2.2 Convective Heat Transfer	17
6.	Mathematical Model	18
	6.1 Bed Material Balance	18
	6.2 Specific Reaction Rates	21
	6.2.1 Reaction Rate Control by First-Order Kinetics and External-Film Diffusion	22

[redacted]

[redacted]

Page

6.2.2 Reaction-Rate Control by External-Film Diffusion and Internal Diffusion 22

6.3 Position of Reaction Interface 28

6.4 Mathematical Solution 28

6.5 Heat Balances 29

7. Computer Solution 30

7.1 Finite-Difference Equations 31

7.2 Computational Procedure 32

7.3 Digital Computer Code 32

8. Differential Bed Tests 33

8.1 Film Transport Constant 33

8.2 Rate Constants for the Oxidation of Carbon Monoxide 41

8.3 Internal Mass-Transport Property 42

8.4 Experimental 42

9. Comparison Between Predicted and Experimental Results 44

9.1 Two-and-one-half-inch diameter Reactor 44

9.2 Five-inch-diameter Reactor 45

9.3 Utility of Mathematical Analyses 45

10. Predictions for Large-Scale Reactors 45

10.1 Potential Problems 52

10.2 Five-inch-diameter Reactor 53

10.2.1 Optimum Operating Conditions for 5-in.-diam Reactor 58

10.2.2 Length of Oxidation Cycle for 5-in.-diam Reactor . 60

10.3 Two-and-one-half-inch-diameter Reactor 60

10.3.1 Optimum Operating Conditions for 2-1/2-in.-diam Reactor 61

[redacted]

Page

10.3.2 Length of Oxidation Cycle for 2-1/2-in.-diam Reactor 66

11. Conclusions and Recommendations 66

11.1 Conclusions 66

11.2 Recommendations 67

12. References 68

13. List of Symbols 70

14. Appendix 73

14.1 Graphite Oxidation Rate-Control by First-Order Kinetics . 73

14.2 Physical Properties of Gases 73

14.2.1 Thermal Conductivity 76

14.2.2 Heat Capacity 76

14.3 Radiative Heat Transfer Constants 78

14.4 Differential Fuel Section Test 81

14.4.1 Rate Constant for CO Oxidation 83

14.4.2 Internal Mass-Transport Property 83

[redacted]

[redacted]

[redacted]

RECOVERY OF URANIUM FROM GRAPHITE FUELS BY OXIDATION AND FLUORINATION

II. USE OF A MATHEMATICAL ANALYSIS OF THE OXIDATION PROCESS IN FIXED BEDS TO PREDICT PROCESS CONDITIONS

C. D. Scott

ABSTRACT

A processing method for recovery of uranium from graphite-uranium fuels by oxygen oxidation followed by fluorination is being investigated. In order to predict effects of operating variables and possibly point out potential problems a mathematical analysis was made of the burning of Kiwi-B-1B-type graphite-uranium fuel in fixed beds as a first step in the reprocessing. Necessary assumptions are listed, and differential and difference equations describing the mathematical model of the system are derived. Results of the analysis revealed several operational problems and were useful in helping to circumvent the problems.

A digital computer program was written for the finite-difference solution of the mathematical representation of the system. This program was prepared for and run on an IBM-7090 computer. The computer solution generates gas composition, gas temperature, fixed-bed fuel temperature, and reactor wall heat flux as a function of time and position in the fixed bed. It was shown that the mathematical model was capable of predicting gas composition and fuel temperature within acceptable limits of experimentally measured values for deep-bed oxidation of Kiwi-B-1B fuel rods.

[redacted]

Problems anticipated with large-scale burning are discussed, and the effects of change in operating parameters were determined by the computer solution. These results indicate that excessive heating and high carbon monoxide content of the gas stream will be problems if operating conditions are not correctly chosen. A range of acceptable operating conditions is predicted from the computer solution for both a 5-in.-diam reactor and a 2-1/2-in.-diam reactor. The length of the optimum, safe oxidation, time without accounting for heat-up and cooling down, was estimated to be 4 hr for the 5-in.-diam reactor and 3-1/2 hr for the 2-1/2-in.-diam reactor.

---

1. INTRODUCTION

A proposed processing method for the recovery of uranium from graphite-uranium fuels consists in the oxidation of the fuel by oxygen to volatilize the carbon, followed by fluorination of the resulting ash by elemental fluorine for uranium removal.[1] The feasibility of both the oxidation and the fluorination steps has been shown on a small engineering scale for Kiwi-B-1B-type graphite-uranium fuel prototype,[2,3] and it is desirable to utilize the small-scale results to predict large-scale operation.

For example, such process variables as gas-phase carbon monoxide concentration and maximum temperature must be controlled within acceptable limits for safe operation, and one must be able to predict these variables for any anticipated operating conditions. This report presents a method

for predicting these variables, based on a mathematical analysis of the system that results in a useful mathematical model which aided in foreseeing and circumventing operational problems. Results of this analysis for oxidation of Kiwi-type graphite fuel rods in a fixed-bed are presented.

This report is the second in a series of reports on the same general topic which have the same main title, Recovery of Uranium from Graphite Fuels by Oxidation and Fluorination, and appropriate subtitles denoting some phase of progress. The first report in the series covered the design and initial operation of an engineering-scale apparatus for Rover fuel.[3]

2. PROCESS FLOWSHEET

A simplified process flowsheet of the system includes a reaction vessel charged with Kiwi-type fuel rods in which the two main processing reactants, oxygen and fluorine, can be introduced (see Fig. 2.1). The reaction vessel must have provisions for external heating so that the oxidation reaction can be initiated (about 700°C) and the fluorination reaction can be made to progress at a suitable rate (about 400°C), and external cooling so that the reaction vessel will not overheat during the oxidation process.

There must also be provision for handling the off-gas from the reactor processing steps. This process is described in more detail in refs 1, 2, and 3.

3. REACTION KINETICS

It is desirable to be able to predict heat generation rates, reaction rates, gas composition, and system temperatures as functions of bed height and run time for the oxygen oxidation of graphite-uranium fuels in fixed

[redacted]

ORNL-DWG 63-4569

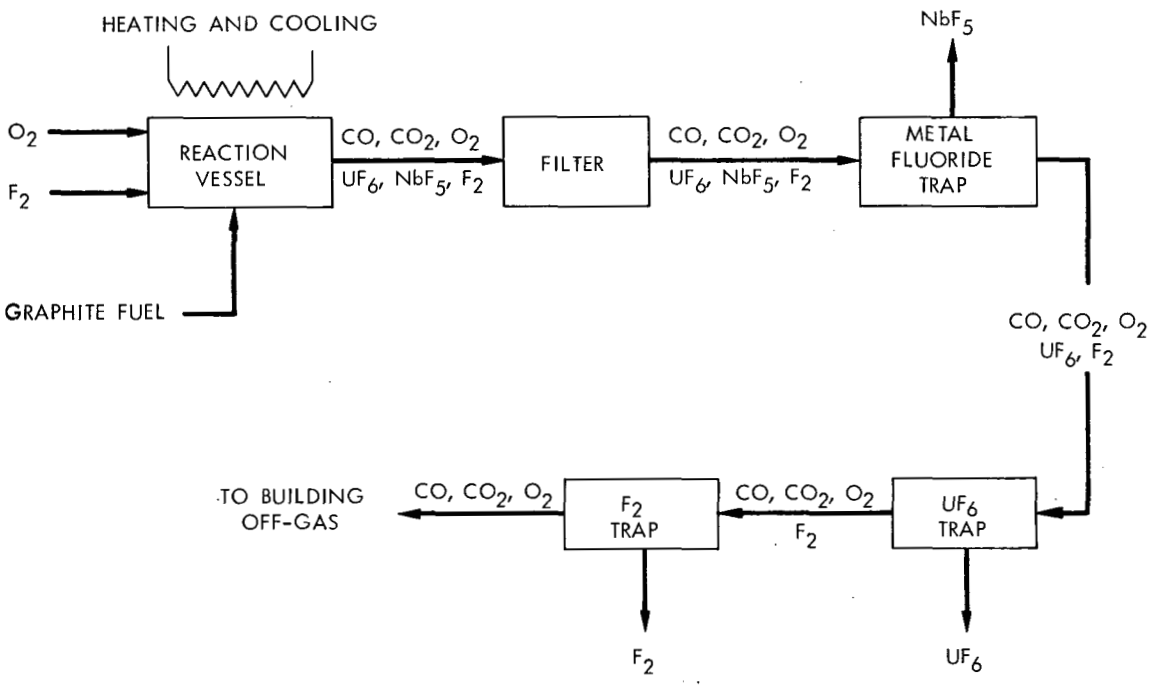

Fig. 2.1. Process Flowsheet for Kiwi-Type Graphite-Uranium Fuel Oxidation and Fluorination Process.

beds. This can be accomplished by considering possible mechanisms of reaction, heat generation, and heat transfer for the process, which will then allow the derivation of differential equations describing an assumed model of the system. This was done specifically for Kiwi-type graphite fuel (for description of the fuel see ref 3); however, the general approach to the problem is usable for other types of graphite-uranium fuels.

3.1 Chemical Reactions

The major chemical reactions that occur in fixed beds of graphite fuels during burning with oxygen are: oxidation of the graphite to carbon monoxide or carbon dioxide,

$$2C + O_2 = 2CO \tag{3.1}$$

$$C + O_2 = CO_2 \; ; \tag{3.2}$$

oxidation of uranium compounds to U_3O_8,

$$\text{uranium compound} + \text{oxygen} = U_3O_8 \; ; \tag{3.3}$$

and oxidation of other metal compounds to their oxides,

$$\text{metal compound} + \text{oxygen} = \text{metal oxide} \; . \tag{3.4}$$

Within the graphite fuel and throughout the reaction system, the oxidation of CO to CO_2 by oxygen can also occur:

$$2CO + O_2 = 2CO_2 \; . \tag{3.5}$$

Since, in the usual graphite fuel, the carbon content predominates (more than 90 mole %), only the oxidation of carbon and carbon monoxide will be considered significant for determining bulk gas-phase composition and heat generation. Therefore, Eqs. (3.1), (3.2), and (3.5) will be considered in more detail.

3.2 Graphite Oxidation

The primary reaction of oxygen with carbon at the carbon reaction site will produce only carbon dioxide at low temperature (less than 500°C), Eq. (3.2), and only carbon monoxide at high temperature (higher than 1000°C), Eq. (3.1).[4] However, the further oxidation of carbon monoxide to CO_2, Eq. (3.5), occurs in the presence of oxygen and is catalyzed by available surface such as the metal oxide ash. Thus, when the kinetics of graphite oxidation is considered, both Eqs. (3.1) and (3.2) must be considered.

Many kinetic mechanisms can control a heterogeneous reaction system such as the reaction of a flowing stream of oxygen with a fixed bed of porous graphite fuel. These include:

1. reaction of the oxygen with graphite at the graphite-oxygen reaction site (assumed to be controlled by a first order reaction),
2. mass transport of the reacting gas from the bulk gas to the solid surface, and
3. mass transport of the reacting gas through the porous solid to a reaction site.

3.2.1 First-Order Kinetics

The reaction of oxygen with graphite at the graphite reaction site can be approximated by a first-order reaction rate dependent upon the oxygen concentrations in the temperature range of 500 to 700°C. The experimental data of Earp and Hill,[5] Dahl,[6] and Currie *et al.*,[7] as presented by Prados[4] was used to obtain a first-order rate equation in which the reaction rate of oxygen with graphite was expressed as

$$R_C = k_1 a C_{O_2} \ , \tag{3.6}$$

where

R_C = rate of oxygen reaction with carbon to form carbon monoxide,

k_1 = rate constant,

a = area available for reaction,

C_{O_2} = bulk gas oxygen concentration.

Available experimental data were correlated to obtain the rate constant in an Arrhenius-type expression (see Appendix 14.1),

$$k_1 = Ae^{-E/RT} \ , \tag{3.7}$$

where

A = constant,

E = activation energy,

R = gas constant,

T = absolute temperature.

The activation energy E was found to be 42.8 Kcal/g-mole of oxygen. The rate constant k_1 is dependent on temperature, and, at reasonably high temperatures (more than 800°C), the rate at the reaction site probably will not be the rate-controlling mechanism if other rate resistances are present.

3.2.2 External Mass Transport

Mass transport of the oxygen from the bulk gas to the external surface of the fuel rod is a reaction rate resistance which may contribute to the control of the C-O_2 reaction. In heterogeneous flow systems such as the graphite-oxygen system, the resistance to "external" mass transport can be approximated by a stagnant gas film surrounding the solid phase through which the oxygen must diffuse. The rate of mass transport is usually expressed by:

$$R = k_g a(C_{O_2}^E) , \tag{3.8}$$

where

k_g = external mass transport rate constant,

a = external surface available for mass transport,

$C_{O_2}^E$ = oxygen concentration on the surface of the solid phase.

The rate constant k_g is a function of the physical properties of the gas and the mass flow rate. Many correlations are available for the mass transfer coefficient for systems similar to this one. The usual correlation is the mass transfer factor J_D as a function of the modified Reynolds number,

where

$$J_D = \frac{k_g \rho}{G} N_{Sc}^{2/3} , \tag{3.9}$$

ρ = gas density,

G = gas mass flowrate,

N_{Sc} = Schmidt number = $\mu/\rho D$,

μ = gas viscosity,

D = molecular diffusivity of the reacting species.

The correlation by Hobson and Thodos[8] was used in this study:

$$J_D = 1.30\ N_{Re}^{-0.45} , \tag{3.10}$$

where

N_{Re} = modified Reynolds number = $d_p G/\mu$,

d_p = diameter of fuel rod.

Combining Eqs (3.9) and (3.10), the mass transfer coefficient can be expressed as:

$$k_g = \frac{1.3G}{\rho} N_{Re}^{-0.45}\ N_{Sc}^{-0.67} . \tag{3.11}$$

3.2.3 Internal Mass Transport

It was found in early experimental work on this system[2,3] that as the graphite-uranium fuel was oxidized in a fixed bed, the resulting ash or metal oxide which was formed tended to adhere to the graphite surface in a layer, and, even after oxidation, the ash remained as a sintered mass closely approximating the shape of the original fuel rod. Thus, if reaction between the graphite in partially reacted fuel and oxygen occurs, the oxygen must diffuse through the porous ash to the graphite reaction site. This "internal" mass transport of the oxygen represents another resistance to the reaction, and it may also contribute to the control of the reaction rate.

In order to further evaluate the internal mass transport effect, the shape of the fuel rods must be known. The Kiwi-B-1B fuel has the form of long cylinders, and they are arrayed vertically in the tubular reactor. If Fick's second law of diffusion holds, the diffusional relationship can be expressed by:

$$\frac{\partial C_{O_2}^{S}}{\partial t} = D^2 \, C_{O_2}^{S} \, , \tag{3.12}$$

where $C_{O_2}^{S}$ is the oxygen concentration in the gas phase within the solid. For any small increment of time and where radial diffusion only is important, the process can be considered to be at steady state. Then Eq. (3.12) becomes:

$$\frac{\partial}{\partial r}\left(r \, \frac{\partial C_{O_2}^{S}}{\partial r}\right) = 0 \, , \tag{3.13}$$

where r represents radial distance within the cylinder.

The general solution to Eq. (3.13) is:

$$C_{O_2}^{S} = A + B \ln r \ , \tag{3.14}$$

where A and B are constants of integration.

If first-order kinetics are not important for reaction rate control at the same time that internal mass transport contributes to reaction rate control, and if the reaction at the reaction site is essentially irreversible, then the following boundary conditions apply:

$$\begin{aligned} r = r_E \qquad & C_{O_2}^{S} = C_{O_2}^{E} \ , \\ r = r_I \qquad & C_{O_2}^{S} = 0 \ , \end{aligned} \tag{3.15}$$

where

r_E = external radius of the fuel rod,

r_I = radius of the reaction interface between ash and unreacted graphite.

After using these boundary conditions in Eq. (3.14), the reaction rate of oxygen with carbon with internal mass transport of the oxygen controlling the reaction rate:

$$C_{O_2}^{S} = C_{O_2}^{E} \frac{\ln\left(\frac{r}{r_I}\right)}{\ln\left(\frac{r_E}{r_I}\right)} \ . \tag{3.16}$$

The oxygen reaction rate with carbon must be equal to the rate of oxygen diffusion to the reaction interface, r_I:

$$R_C = 2\pi r_I \alpha D \left(\frac{\partial C_{O_2}^{S}}{\partial r}\right)_{r=r_I} \ , \tag{3.17}$$

where

α = effective solid-phase porosity,

D = oxygen molecular diffusivity.

From Eq. (3.16) it can be shown that

$$\left(\frac{\partial C_{O_2}^S}{\partial r}\right)_{r=r_I} = \frac{C_{O_2}^E}{r_I \ln \frac{r_E}{r_I}} ; \tag{3.18}$$

therefore,

$$R_C = \left(2\pi\alpha D C_{O_2}^E / \ln \frac{r_E}{r_I}\right). \tag{3.19}$$

3.3 Carbon Monoxide Oxidation

If CO is the product of the graphite-oxygen reaction, the kinetics of the oxidation of the CO must also be considered since this represents additional oxygen usage and it will influence the content of explosive gas in the system. There is evidence that the CO-O_2 reaction, Eq. (3.5), is surface catalyzed and dependent on both the oxygen and CO gas-phase concentration.[9,10] Although the exact order of dependence on the reaction rate of CO with oxygen on the CO or oxygen concentration has not been established for the conditions of this system, it was assumed that the rate could be expressed by:

$$R_{CO} = K_c C_{O_2}^S C_{CO}^S , \tag{3.20}$$

where

K_c = the rate constant dependent on temperature and surface area,

R_{CO} = the rate of oxygen reacting with CO,

$C_{O_2}^S$, C_{CO}^S = the gas-phase concentration of O_2 and CO within the solid at the reaction site.

Although there will probably be some gas-phase, homogeneous reaction of CO and oxygen, the controlling rate of reaction will occur on available surface (the ash surface should be a good catalyst for this reaction).

4. PHYSICAL PROPERTIES

Several physical properties of the fixed-bed, graphite-fuel oxidation system, for both gas and solids, must be known or assumed to permit a mathematical solution of the system. These are discussed below.

4.1 Gas Properties

Physical properties of the system relating to the gas phase which must be known are average molecular weight M, molar density ρ, thermal conductivity k_T, heat capacity C_P, molecular diffusivity of the reacting gas D, viscosity of the reacting gas μ, convective heat transfer coefficient for both the gas-fuel interface and the gas-reactor wall interface h_r and h_w, film mass transfer coefficient for oxygen transfer to the fuel surface k_g, and volumetric flow rate of the gas F. These properties also will allow calculation of the modified Reynolds number N_{Re}, Schmidt number N_{Sc}, and Prandtl number N_{Pr}, which are useful in determining transport coefficients.

For the gas mixture, it was assumed that a physical property was a linear combination of the properties of the individual gases in the mixture. All gases were assumed to be perfect gases, and the mixture was assumed to be ideal. Thus Dalton's Law would apply:

$$P_i = \frac{x_i RT}{V}, \tag{4.1}$$

where

p_i = partial pressure of the ith component,

x_i = mole fraction of the ith component,

R = gas constant,

T = absolute temperature,

v = specific molar volume of the gas mixture.

Molar density of the gas mixture was obtained from the equation of state of an ideal gas:

$$\rho = \frac{1}{v} = \frac{p}{RT} . \tag{4.2}$$

The thermal conductivity for the individual gases k_{T_i} were correlated in linear expressions:

$$k_{T_i} = A_i T_g + B_i ; \tag{4.3}$$

and the thermal conductivity of the gas mixture containing n components was :

$$k_T = \sum_{i=1}^{n} x_i \, k_T , \tag{4.4}$$

where

i = i^{th} component,

T_g = absolute gas temperature,

A and B = empirical constants.

Heat capacity for the individual gas in the gas mixture C_{p_i} was correlated in the conventional expression:

$$C_{p_i} = a_i + b_i T_g + c_i T_g^{-2} ; \tag{4.5}$$

and heat capacity for the gas mixture was obtained by:

$$C_p = \sum_{i=1}^{n} x_i \, C_{p_i} . \tag{4.6}$$

The individual gas-phase properties mentioned were obtained from conventional correlations or data from literature sources and are presented in Appendix 14.2.

4.2 Graphite-Uranium Fuel Properties

Physical properties of the fuel-phase in the fixed bed-oxidation which are needed for a mathematical analysis of the system are: shape of the fuel rods, chemical composition of the fuel rod, effective graphite density in the fuel phase, and effective porosity of the oxidation ash formed during oxidation if the ash is sintered in place.

The fuel of major interest for this report is Kiwi-B-1B-type graphite-uranium fuel, which will be used in the Rover Project. The fuel is available in the form of long cylinders, and for simplicity, it is assumed that the fuel rod is solid and that it contains only graphite or materials that can be given a molar equivalent to graphite for purposes of reaction rate and heat of reaction. The equivalent graphite density in this assumed solid fuel rod is 0.104 g-mole per cubic centimeter of fuel. (For a complete description of the Kiwi-B-1B-type fuel, see ref. 3.)

The effective porosity for oxygen mass transport in the oxidation-ash phase α was determined to be 0.085 from a differential bed experiment (see Appendix 14.4). The fuel rods were placed into the reaction vessel as long pieces standing vertically.

5. HEAT GENERATION AND HEAT TRANSFER

If the specific reaction rates, reactor wall temperature, gas temperature, fuel rod temperature, and fuel geometry are known for a section of the fixed bed of graphite fuel being oxidized by a flowing stream of oxygen-bearing gas, the heat transfer to the wall and gas, change in fuel

temperature distribution and change in gas temperature can be approximated for a short time if the controlling heat transfer mechanisms are known.

5.1 Heat Generation

Heat is generated by the chemical reactions shown in Eqs. (3.1), (3.2), and (3.5). The heats of reaction for these two reactions can be determined from existing thermodynamic data,[11] and they remain almost constant over the temperature range of interest.

5.2 Heat Transfer Mechanisms

Heat transfer from the fuel rods will occur in two main ways: by radiation and by convection.

5.2.1 Radiative Heat Transfer

Radiative heat transfer occurs between the various fuel rods and other fuel rods and the reactor wall. It was assumed that under the conditions of this system, radiative heat transfer to or from the gas phase was negligible.

The equation for net radiative heat transfer between two bodies can be expressed as:

$$q_{12} = \sigma A F_{12}(\epsilon\, T_1^4 - T_2^4\, \alpha) \ , \tag{5.1}$$

where

q_{12} = net heat transfer from surface 1 to surface 2,

σ = Stefan-Boltzmann constant,

A = radiative heat transfer area of surface 1,

F = view factor (shape or geometry factor),

T_1, T_2 = absolute temperature of surfaces 1 and 2,

ϵ = emissivity of surface 1,

α = absorptivity of surface 2.

For this system, the emissivity and absorptivity of the surfaces involved in radiation were assumed to be unity and the equation simplifies to:

$$q_{12} = K_{12}(T_1^4 - T_2^4) \ , \tag{5.2}$$

where K_{12} is the radiative heat transfer coefficient.

Only two radial positions in the fixed bed of fuel were considered for the heat transfer problem: (1) the center fuel rod which should be at a maximum system temperature, and (2) the outside fuel rods. All radiative heat transfer was assumed to be radial only, and radiative heat transfer to the walls occurred from the outside rods only. In tightly arrayed reactors this will be a good assumption; however, for loose arrays where the center rods can "see" appreciable portions of the walls, the radiative heat transfer coefficient should be adjusted.

These assumptions allow the radiative heat transfer phenomena to be described by only two equations and three temperatures. Radiative heat transfer from the center rod will be:

$$q = K_c(T_c^4 - T_o^4) \ ; \tag{5.3}$$

and radiative heat transfer from outside rods will be:

$$Nq = K_o(T_o^4 - T_w^4) \ , \tag{5.4}$$

where

q = heat generated in one rod,

N = number of fuel rods in array,

K_c, K_o = effective radiative heat transfer coefficients for center rod and outside rods,

T_c, T_o, T_w = temperature of center rod, outside rods, and reactor wall. The method for determining the values for the effective radiative heat transfer coefficients are shown in Appendix 14.3.

5.2.2 Convective Heat Transfer

Generated heat from the fuel rod oxidation will also be transferred from the fuel rods by convective heat transfer to the flowing gas stream, and the gas will lose heat to the reactor wall by convecting heat transfer. Convective heat transfer from a solid surface to a flowing gas can be described by an equation of the following form:

$$q = hA(T_s - T_g) \ , \tag{3.5}$$

where

T_s, T_g = temperature of the surface and gas,

h = convection heat transfer coefficient.

Several correlations for convective heat transfer coefficients are available for systems similar to the fixed-bed graphite oxidation. These correlations usually result in the convective heat transfer coefficient being dependent on some of the physical properties of the gas, notably the gas mass flow rate, gas heat capacity, Reynolds number, thermal conductivity, Prandtl number, and the shape of the system. For heat transfer from a fuel rod to the gas, an expression developed by Satterfield and Resnick[12] was used:

$$h_r = 0.992\ C_p G(N_{Re})^{-0.34}(N_{Pr})^{-0.667} \ . \tag{5.6}$$

For the convective heat transfer coefficient for heat transfer from the gas to the reactor wall, an expression developed by Hanrattry[13] was used:

$$h_w = \frac{0.55\ k_T}{r_w}(N_{Re})^{0.5}(N_{Pr})^{0.5} \ , \tag{5.7}$$

where r_w is the radius of the reactor wall.

6. MATHEMATICAL MODEL

The reaction system can be represented by a set of differential or difference equations which describe the reaction-rate-controlling processes and material balance relationships. These equations constitute the mathematical model of the system, and a solution of the set of equations results in a complete description of the system if the original assumptions are correct. Simple heat balance equation will then allow determination of the system temperature.

6.1 Bed Material Balance

Several assumptions were made to simplify the equations describing the bed material balance:

1. The fixed bed is composed of a vertical array of cylindrical fuel rods contained in a cylindrical reactor.
2. All physical and chemical properties of the gas-phase are independent of radial position in the bed.
3. Diffusion of gas components in the direction of flow is negligible.
4. Inlet gas properties and flow rate are constant.
5. Changes in gas-phase physical and chemical properties for any small increment of bed height are negligible.
6. The gas holdup in the fuel rod void volume is negligible.
7. Specific chemical reaction rate is independent of radial position.
8. Changes in the chemical or physical properties of the solids at a point in the fixed bed occur as a step change at the end of a differential time element.

9. Changes in the flowing gas stream as a result of reaction or heat transfer occur in the fixed bed as a step change at the end of an increment of bed height but before the gas enters the next increment of bed height.

10. The system pressure is constant throughout the reactor.

The bed material balance for each gas component must be considered separately. A rigorous derivation of the differential material balance of the gas component (such as that by Klotz[14]) will not be possible for this system since several of the properties of the gas-phase, such as volumetric flow rate and temperature, do not remain constant with bed position and reaction time; therefore, a simplified material balance relationship will be used which meets the requirements of the listed assumptions.

Consider a differential volume of the fixed bed that results from a differential height of the bed dz at a distance z from the gas entrance (Fig. 6.1). The gas enters the differential section at a volumetric flow rate of F and an oxygen concentration of $(C_{O_2})_z$. Gas leaves the differential section at a flow rate of (F + dF) and at an oxygen concentration of $(C_{O_2})_{z+dz}$. Oxygen is removed from the gas stream in the differential volume by its reaction with graphite to form CO, R_C, or with carbon monoxide to form CO_2, R_{CO}. Using the law of conservation of mass and for a unit length of time, the material balance will be :

$$F(C_{O_2})_z - (F + dF)(C_{O_2})_{z+dz} = N(R_C + R_{CO})\ dz\ , \qquad (6.1)$$

where the reaction rates R_C and R_{CO} are expressed in rate of oxygen reaction per unit height of an individual fuel rod, and N is the total number of fuel rods in the reactor.

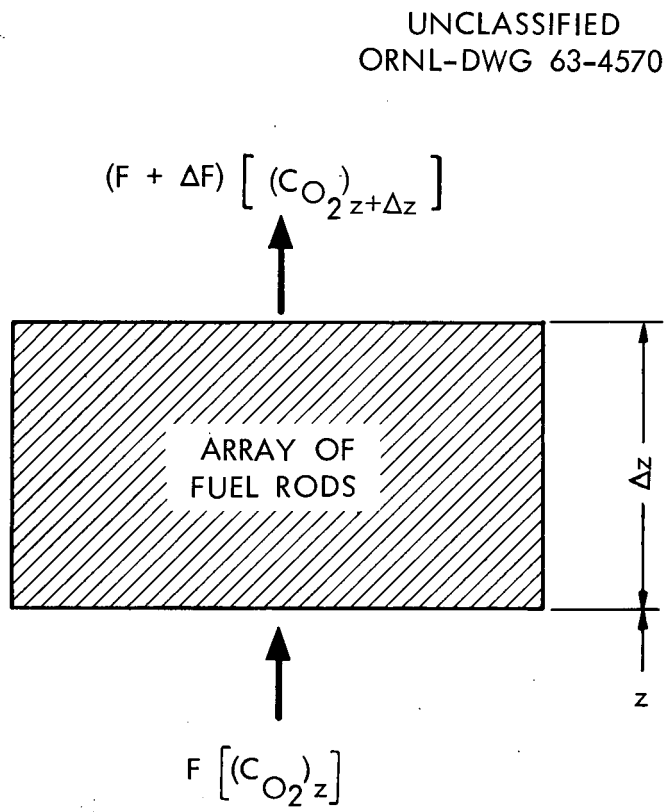

Fig. 6.1. Section of Differential Volume in the Fixed Bed of Fuel.

Equation (6.1) may be rearranged to give:

$$(C_{O_2})_{z+dz} = \frac{F(C_{O_2})_z - N(R_C + R_{CO})\ dz}{(F + dF)} . \tag{6.2}$$

The change in volumetric flow rate, dF, must also be evaluated. Since the pressure is constant, the change in flow rate will result from the generation of CO (reaction 3.1). Therefore, dF can be expressed by:

$$dF = \frac{(R_C - R_{CO})}{\rho}\ dz , \tag{6.3}$$

where ρ is the total gas density at the conditions of the system. After $(C_{O_2})_{z+dz}$ is determined from Eqs. (6.2) and (6.3), to get the true volumetric concentration of oxygen, the change in temperature must also be considered and the change in volume of the gas due to temperature change can be found by use of the ideal gas law.

Use of the oxygen mole fraction x_{O_2} instead of the concentration is somewhat simpler for finite difference calculations. Equation (6.2) can be put in the form in which the mole fraction is used:

$$(x_{O_2})_{z+dz} = \frac{\rho F(x_{O_2})_z - N(R_C + R_{CO})\ dz}{\rho(F + dF)} . \tag{6.4}$$

Similar material balance expressions can be determined for both carbon monoxide and carbon dioxide:

$$(x_{CO})_{z+dz} = \frac{\rho F(x_{CO})_z + 2N(R_C - R_{CO})\ dz}{\rho(F + dF)} , \tag{6.5}$$

$$(x_{CO_2})_{z+dz} = \frac{\rho F(x_{CO_2})_z + 2NR_{CO}\ dz}{\rho(F + dF)} , \tag{6.6}$$

where dF is still defined by Eq. (6.3).

6.2 Specific Reaction Rates

In order to use the material balance equations, it is necessary to

have expressions for the specific reaction rates R_C and R_{CO}, which relate them to the gas-phase composition and properties of the fuel-rod phase.

6.2.1 Reaction Rate Control by First-Order Kinetics and External Film-Diffusion

For the case of reaction rate control by first order kinetics and the external, stagnant gas film [Eqs. (3.6) and (3.8)], the two rate resistances represented by the rate constants k_1 and k_g can be combined to give an over-all rate constant k_o by:

$$\frac{1}{k_o} = \frac{1}{k_1} + \frac{1}{k_g} , \tag{6.7}$$

or

$$k_o = \frac{k_1 k_g}{k_1 + k_g} . \tag{6.8}$$

The specific reaction rate will then be:

$$R = \frac{2\pi r_I k_1 k_g}{k_1 + k_g} C_{O_2} , \tag{6.9}$$

where R is the over-all rate of reaction of oxygen with graphite to CO_2, and

$$R = R_C = R_{CO} . \tag{6.10}$$

6.2.2 Reaction-Rate Control by External-Film Diffusion and Internal Diffusion

In the region where first-order kinetics do not control, only external diffusion and internal diffusion resistances are considered. However, since CO will be the primary reaction product at the O_2-C reaction site, the O_2-CO reaction [Eq. (3.5)] will also be occurring throughout the zone of internal oxygen diffusion (in the oxidation ash). This makes a rigorous solution of the internal diffusion problem very difficult since

the CO-O_2 reaction is a second order reaction depending on two different gas species.

Danckwerts, as presented by Crank,[15] gave an approximate method of solution for the case of diffusion with first-order reaction occurring, however, addition of the second order relationship with simultaneous diffusion of two species, oxygen and CO, in opposite directions makes his solution unusable. One can approximate this system by separating the diffusion problem from the second-order kinetics problem and considering only the diffusion of one species, oxygen, since molecular diffusivities of all of the species are comparable in this system. This can be done by assuming that the CO-O_2 reaction occurs only in a hypothetical reaction shell of differential thickness at the outer surface of the fuel rod. In this reaction shell or zone, the oxygen concentration will be that of the oxygen after diffusing through the external gas film and the CO concentration will be that of the CO at the O_2-C reaction site. Further, the surface area available for the surface-catalyzed O_2-CO reaction in the reaction zone will be that surface of the outside of the fuel rod plus that surface area in the oxidation ash built up on the fuel rod. This approximation should be fairly realistic in the early stages of the reaction when the O_2-C reaction site is close to the external rod surface.

The physical model which results from these assumptions is shown in Fig. 6.2. The fuel rod, of radius r_E, is surrounded by a stagnant gas film, or radius r_F, and immediately surrounding the outer surface of the fuel rod is the hypothetical O_2-CO reaction zone of radius r_H with $r_H \approx r_E$. The reaction interface or carbon-ash interface is at a radius of r_I and the combustion ash is in the space between r_I and r_E.

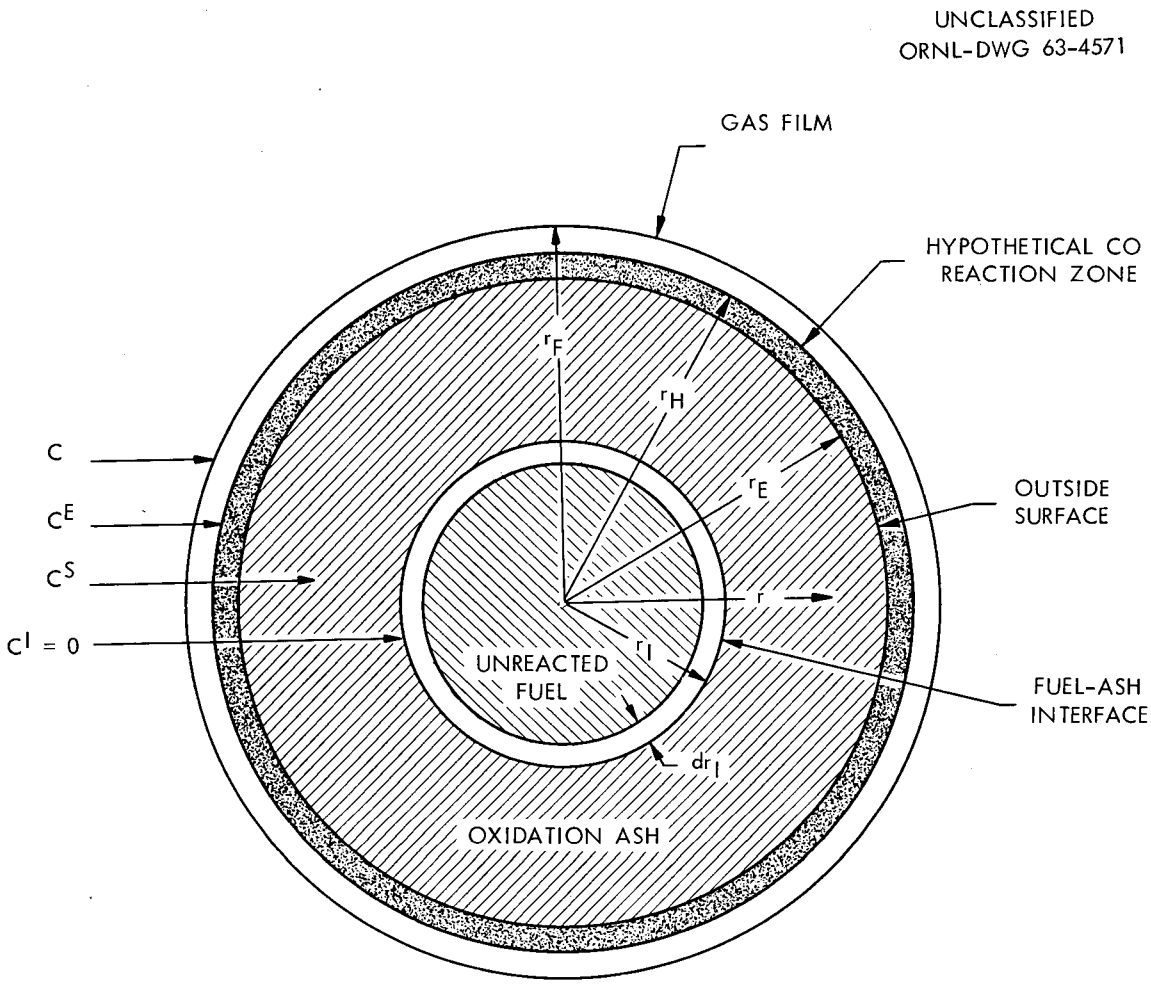

Fig. 6.2. Section of the Cylindrical Model Used to Describe the Reaction of O_2 with Graphite-Uranium Fuel Rods.

The fuel-rod gas composition can also be qualitatively shown. The oxygen concentration will decrease from the bulk gas value, C_{O_2} to $C^E_{O_2}$ due to the external gas film resistance $(r_F - r_H)$ (see Fig. 6.3). It will remain constant in the hypothetical reaction zone $(r_H - r_E)$, and then there will be a predictable concentration gradient from r_E to r_I due to the internal pore diffusion resistance in the ash. At the reaction site, the oxygen concentration will go to zero.

Carbon monoxide concentration will be constant from the reaction site to the hypothetical reaction zone $(r_I - r_E)$ where it decreases to its bulk gas-phase value $(r_E - r_H)$. Carbon dioxide and inert gas concentrations will be then obtained by material balance and stoichiometry considerations.

The reaction rate of oxygen with CO in the hypothetical reaction zone can be expressed by:

$$R_{CO} = \left[k_{c_1} + k_{c_2}\,(r_E^2 - r_I^2)\right]\, C^E_{O_2} C^I_{CO}\,, \tag{6.11}$$

where

k_{c_1} = reaction rate constant dependent on available external surface of fuel rod,

k_{c_2} = reaction rate constant dependent on available internal surface in the ash,

C^E = gas concentration at external surface of fuel rod,

C^I = gas concentration at reaction interface.

The rate of reaction of the graphite with oxygen R_C is dependent on the diffusion of oxygen from the bulk gas phase to the reaction site at r_I. It was shown in Sec 3 that

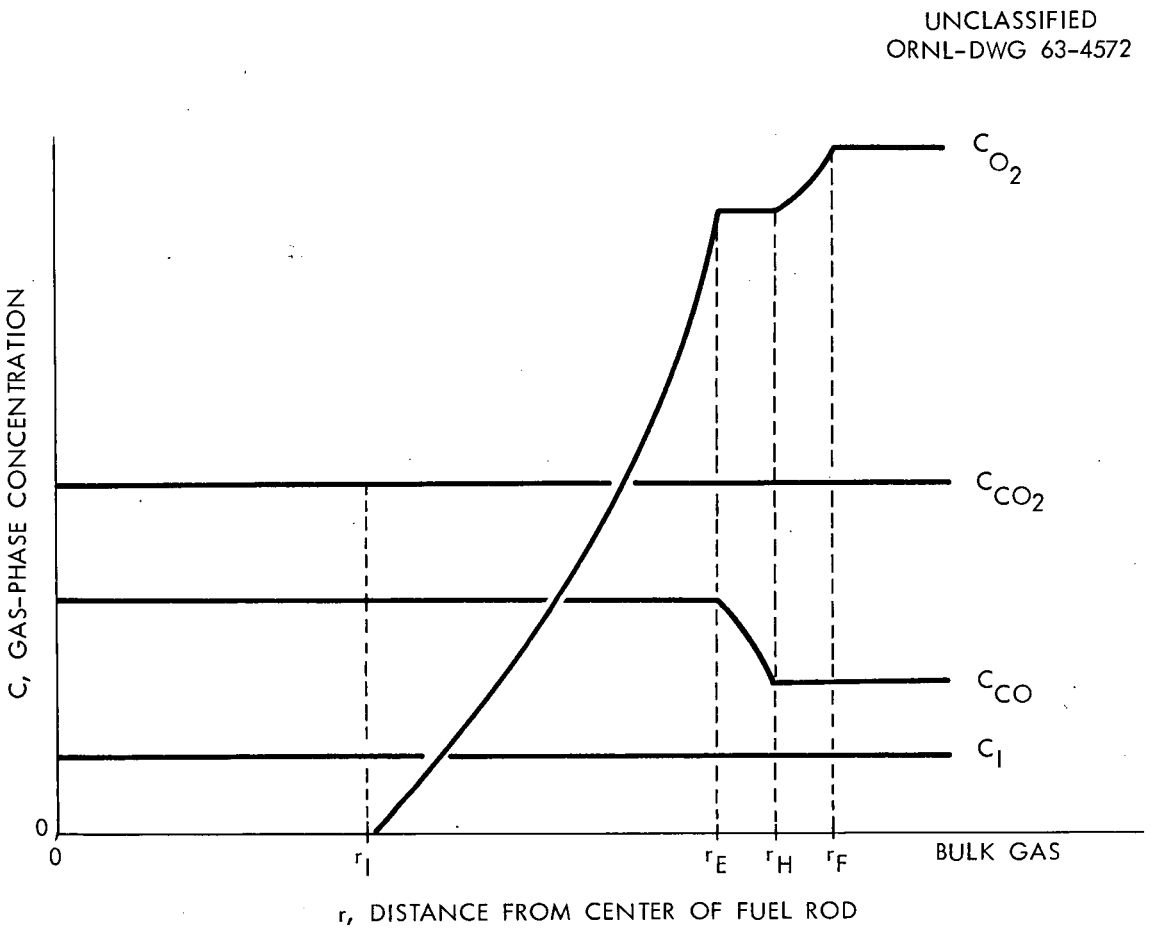

Fig. 6.3. Gas-Phase Concentration Gradients as Predicted by the Mathematical Model.

$$R_C = \frac{2\pi\alpha D C_{O_2}^E}{\ln \frac{r_E}{r_I}} . \tag{6.12}$$

Total oxygen reaction rate must equal the total for graphite oxidation R_C and CO oxidation R_{CO}:

$$R = R_C + R_{CO} . \tag{6.13}$$

Substituting Eqs. (6.11) and (6.12) into Eq. (6.13) gives:

$$R = \frac{2\pi\alpha D C_{O_2}^E}{\ln \frac{r_E}{r_I}} + \left[k_{c_1} + k_{c_2} (r_E^2 - r_I^3) \right] C_{O_2}^E C_{CO}^I . \tag{6.14}$$

The CO concentration at the reaction interface will be the difference between the total gas concentration or gas molar density and the CO_2 and inert gas concentrations. Using the perfect gas law, this gives:

$$C_{CO}^I = \frac{P}{RT} - C_{CO_2} - C_I , \tag{6.15}$$

where

T = temperature in fuel rod,

R = gas constant,

P = total pressure.

Equation (6.14) becomes:

$$R = \left\{ \frac{2\pi\alpha D}{\ln \frac{r_E}{r_I}} + \left[k_{c_1} + k_{c_2} (r_E^2 - r_I^2) \right] \left(\frac{P}{R\,T} - C_{CO_2} - C_I \right) \right\} C_{O_2}^E . \tag{6.16}$$

Equations (3.8) and (6.16) can be combined to obtain an expression for $C_{O_2}^E$ in terms of the oxygen bulk gas composition, C_{O_2}:

$$C_{O_2}^{E} = \frac{2\pi r_E k_g C_{O_2}}{\left(\frac{2\pi\alpha D}{\ln \frac{r_E}{r_I}}\right) + \left\{\left[k_{c_1} + k_{c_2}\left(r_E^2 - r_I^2\right)\right]\left(\frac{P}{R\ T} - C_{CO_2} - C_I\right)\right\} + 2\pi r_E k_g} \ . \tag{6.17}$$

Equations (6.16) and (6.17) give the specific reaction rate of oxygen for the case of external and internal diffusion of oxygen controlling the rate of its reaction with graphite. Equations (6.14) and (6.12) with Eq. (6.17) give the specific reaction rates for the O_2-C reaction and the O_2-CO reaction.

6.3 Position of Reaction Interface

The specific reaction rates are expressed in terms of the position of the reaction interface r_I. Since this interface position will move with time because of the O_2-C reaction, it is necessary to derive an expression for its movement. This can be done by equating the carbon reaction rate R_C to the movement of the interface which will satisfy the stoichiometry of Eq. (3.1):

$$2R_C = -\ 2\pi b r_I \frac{dr_I}{dt} \ , \tag{6.18}$$

where b is molar density of graphite in the fuel rod phase. Rearranging Eq. (6.18):

$$\frac{dr_I}{dt} = -\ \frac{R_C}{\pi b r_I} \ . \tag{6.19}$$

6.4 Mathematical Solution

The necessary partial differential equations are now available for a mathematical solution of the proposed mathematical model. Simultaneous solution of Eqs. (6.4), (6.5), (6.6), (6.7), (6.8), (6.19), or (6.4),

(6.5), (6.7), (6.16), (6.17), and (6.19) will result in the mathematical solution of the system and allow prediction of the O_2-C and O_2-CO reaction rates at any point in the reactor as a function of time. This will also allow prediction of the bulk gas-phase composition as a function of time and bed position.

6.5 Heat Balances

If the reactor wall temperature T_w, inlet gas temperature T_g, reaction rates R_C and R_{CO}, past temperature history of fuel rods, and shapes of the fuel rods are known for a differential section of the bed, then heat transfer to the wall, the fuel rod temperature, and the change in gas temperature can be determined from heat balance equations. As mentioned before, the mechanisms of heat transfer considered are radiant transfer from fuel rod to fuel rod and fuel rod to reactor wall, and convective transfer from fuel rod to gas and gas to reactor wall.

The heat balance around the center fuel rod per unit time will be:

$$q = K_c(T_c^4 - T_o^4) + h_r(T_c - T_g) + \frac{C_{p_s}}{\Delta t}(T_c - T_c^o) , \qquad (6.20)$$

where

q = specific heat generated by chemical reactions in one fuel rod,

C_{p_s} = heat capacity of the fuel rod,

T_c^o = temperature of center fuel rod prior to the time increment of interest.

Heat balance around all the fuel rods will be:

$$qN = K_o(T_o^4 - T_w^4) + Nh_r(T_o - T_g) + \frac{C_{p_s} N}{\Delta t}(T_o - T_o^o) . \qquad (6.21)$$

In Eq. (6.21), the temperature of the outside rods, T_o, was used to

approximate the temperature of all of the rods for purposes of the heat balance. Equations (6.20) and (6.21) can be solved simultaneously for values of T_c and T_o.

A heat balance around the gas in the differential section of the reactor results in the following expression for change in the gas temperature as it passes through the differential bed section:

$$\Delta T_g = \frac{Nh_r(T_o - T_g) - h_w(T_g - T_w)}{C_p F} . \tag{6.22}$$

Finally the heat flux to the reactor wall Q_w, can be determined by the amount of heat transferred by radiation and convection:

$$Q_w = h_w(T_g - T_w) + K_o(T_o^4 - T_w^4) . \tag{6.23}$$

7. COMPUTER SOLUTION

It is desirable to solve the differential equations representing the mathematical model of the reaction system and the algebraic expressions for temperature and wall heat flux so that the gas-composition and temperature relationships will be known as functions of bed position and time for any set of operating conditions in the process of burning fixed beds of graphite-uranium fuels.

The mathematical solution is by a digital computer, utilizing a finite-difference technique in which the equations are solved for successive differential bed sections, which allows establishment of the bed profile of gas composition and temperature. Then, by use of an iterative technique the bed profile can be re-established for additional increments of reaction time.

7.1 Finite-Difference Equations

The differential equations which have been transformed into finite difference form are shown below.

Material balance equations:

$$x_{O_2,m+1,n} = \left[\frac{\rho F x_{O_2} - N(R_C + R_{CO})\ \Delta z}{\rho(F + \rho F)}\right]_{m,n}, \tag{7.1}$$

$$x_{CO,m+1,n} = \left[\frac{\rho F x_{CO} + N(R_C - R_{CO})\ \Delta z}{\rho(F + \Delta F)}\right]_{m,n}, \tag{7.2}$$

$$x_{CO_2,m+1,n} = \left[\frac{\rho F x_{CO_2} + 2NR_{CO}\Delta z}{\rho(F + \Delta F)}\right]_{m,n}, \tag{7.3}$$

where

$$\Delta F_{m,n} = \left[\frac{(R_C - R_{CO})\Delta z}{\rho}\right]_{m,n}. \tag{7.4}$$

Specific reaction rates (first order-film diffusion):

$$R_{m,n} = \left[\left(\frac{2\pi r_I k_1 k_g}{k_1 + k_g}\right) \rho x_{O_2}\right]_{m,n}, \tag{7.5}$$

$$R_{C,m,n} = R_{CO,m,n} = (R_{m,n})/2\ . \tag{7.6}$$

Specific reaction rates (diffusion):

$$C^E_{O_2,m,n} = \left[\frac{\beta\pi r_E k_g C_{O_2}}{\left(\frac{2\pi\alpha D}{\ln \frac{r_E}{r_I}}\right) + \left\{\left[k_{c_1} + k_{c_2}(r_E^2 - r_I^2)\right]\left(\frac{P}{RT} - C_{CO_2} - C_I\right)\right\} + 2\pi r_E k_g}\right]_{m,n}, \tag{7.7}$$

$$R_{C,m,n} = \left[\frac{2\pi\alpha D C^E_{O_2}}{\ln \frac{r_E}{r_I}}\right]_{m,n}, \tag{7.8}$$

$$R_{CO,n,m} = \left[k_{c_1} + k_{c_2}\left(r_E^2 - r_I^2\right)\right]\left(\frac{P}{RT} - C_{CO_2} - C_I\right)_{m,n} C^E_{O_2,m,n} , \qquad (7,9)$$

$$R_{m,n} = R_{C,m,n} + R_{CO,m,n} . \qquad (7.10)$$

Movement of reaction interface:

$$\Delta r_{I,m,n} = - \left[\frac{R_{C\Delta t}}{\pi b r_I}\right]_{m,n} . \qquad (7.11)$$

The subscript m denotes a reactor height increment of size Δz in the fixed bed. Addition of one to the subscript, m+1, indicates a bed-height increment Δz further up the bed from the mth position. Similarily, the second subscript (n) denotes the time increment.

7.2 Computational Procedure

The finite-difference equations (7.1-7.11) and the heat balance equations (6.20-6.23) were the basis for the computer solution of the mathematical model. The finite difference solution was started at time equal to Δt at the entrance point of the gas, where initial conditions were known. This allowed the computation of values of interest at a point Δz further in the bed. This procedure was then repeated until the end of the bed was reached. All the gas composition and temperature profiles in the bed were stored for future use. Another time increment, Δt, was then taken, and, with initial conditions and previous bed profile conditions, another transit of the bed was made. Bed profile values were periodically recorded.

7.3 Digital Computer Code

The computer code was written for the IBM 7090 digital computer located at the Computer Center of the Oak Ridge Gaseous Diffusion Plant.

Automatic coding system used was 7090 FORTRAN. The flow diagram for the computer code is shown in Fig. 7.1, and the resulting 7090 FORTRAN source program is shown in Fig. 7.2. Format of the computer code output is shown in Fig. 7.3.

8. DIFFERENTIAL BED TESTS

In order to use the computer solution of the assumed mathematical model, it was necessary to have values for the reaction rate constants and the mass transport properties of oxygen in both the gas phase and solid phase. Some of these values can be estimated from existing correlations; however, experimentally measured values are more desirable.

If a differential section of fuel rod (full diameter but short height) is exposed to high temperature and an oxygen atmosphere, the resulting reaction rates of oxygen with graphite and CO in the differential element will be the same as a differential element in a deep bed.

The derived differential equations for reaction rate can then be used with the experimental data from differential element tests to establish reaction rate constants.

8.1 Film Transport Constant

At the beginning of a differential element test, the rate of reaction of oxygen with graphite will depend upon the mass transport of oxygen across the external film and the first-order kinetics at the reaction site. If the first-order kinetics contribute to reaction control, the graphite-oxygen reaction can occur throughout a significant portion of the fuel rod rather than at the fuel-rod exterior surface. If low Reynolds numbers are used to ensure a high film diffusion resistance and if the

UNCLASSIFIED
ORNL-DWG 63-4573

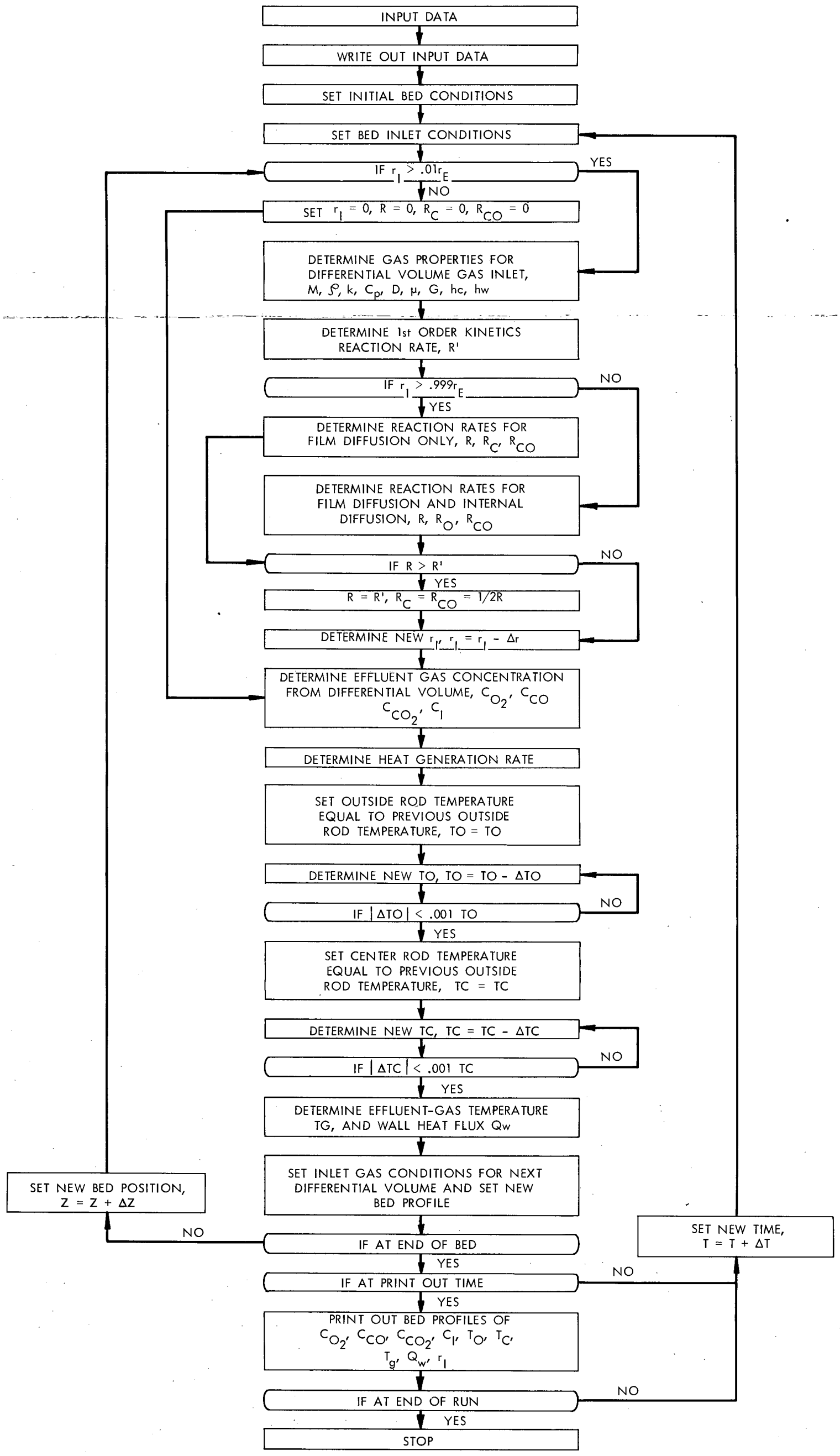

Fig. 7.1. Flow Diagram for the Computer Source Program for the Finite Difference Solution of the Mathematical Model.

```
      DIMENSION CO2(800),CCO(8000),CCO2(800),CI(800),TG(800),TO(800),TC(
     1800),QW(800),R(800),HT(800)
    1 READ INPUT TAPE 10,1001,NC,N1,N2,N3,A1,A2,A3,A4,
     1A5,A6,A7,A8,A9,A10,A11,A12,A13,A14,A15,A16,A17,
     2A18,A19,A20,A21
 1001 FORMAT(I10/I10/I10/I10/(E10.4))
    2 WRITE OUTPUT TAPE 9,1002,NC,A1,A2,A3,A4,A5,A6
 1002 FORMAT(86H1                                        FIXED-BED GRAPHITE-UR
     1ANIUM FUEL OXIDATION BY OXYGEN/80H0
     2        TEMPERATURE AND GAS COMPOSITION PROFILES/69H0
     3                                    COMPUTER CODE NUMBERI4/1H0/65H0
     4                                                      INPUT DATA/4
     53H0                    HEIGHT INCREMENT (A1)=E10.4,37H
     6  TIME INCREMENT (A2)    =E10.4/43H0                    REACTOR RADI
     7US (A3)    =E10.4,37H                NUMBER OF RODS (A4)   =E10.4/43H
     80                    CO RATE CONST KI (AS) =E10.4,37H
     9CO RATE CONST K2 (A6) =E10.4)
    3 WRITE OUTPUT TAPE 9,1003,A7,A8,A9,A10,A11,A12,A13,A14,
     1A15,A16,A17,A18
 1003 FORMAT(43H0                    PRESSURE (A7)          =E10.4,37H
     1          INITIAL O2 FR (A8)     =E10.4/43H0                    INIT
     2IAL CO FR (A9)     =E10.4,37H               INITIAL CO2 FR (A10)   =E
     310.4/43H0                    INITIAL INERT FR (A11)=E10.4,37H
     4        INERT MOL WT (A12)     =E10.4/43H0                    INITIA
     5L FLOWRATE (A13)=E10.4,37H               INITIAL GAS TEMP (A14)=E10
     6.4/43H0                    INITIAL WALL TEMP(A15)=E10.4,37H
     7      WALL TEMP (A16)        =E10.4/43H0                    RAD CONS
     8TANT KO (A17) =E10.4,37H               RAD CONSTANT KC (A18) =E10.4
     9)
    4 WRITE OUTPUT TAPE 9,1004,A19,A20,A21,N1,N2,N3
 1004 FORMAT(43H0                    KIN CONSTANT A (A19)   =E10.4,37H
     1          KIN CONSTANT E/R (A20)=E10.4/43H0                    INTE
     2RFACE FR (A21)     =E10.4,37H               NO OF HT INCR (NI)     =I
     310/43H0                    TIME INC PER PR (N2)   =I10,37H
     4    PRINT OUT PER RUN (N3)=I10)
  100 DO199M=1,N1
  101 R(M)=A21
  102 ZM=M
  103 HT(M)=ZM*A1
  104 TG(M)=A15
  105 TO(M)=A15
  106 TC(M)=A15
  199 CONTINUE
    5 B1=A7/82.06
    6 82=3.14*A3*A3
    7 B3=6.28*A3
    8 B4=A2/0.295
    9 B5=1.48/A2
```

Fig. 7.2. FORTRAN Source Program for the Finite Difference Solution of the Mathematical Model.

```
 10 B6=(A13*A14*2.68)/A7
 11 B7=(A16**4.0)
200 DO299K1=1,N3
300 DO399K2=1,N2
301 BO2=A8
302 BCO=A9
303 BCO2=A10
304 BI=A11
305 BTG=A14
306 BF=B6
400 DO499M=1,N1
401 IF(0.01-R(M))410,402,402
402 R(M)=0.0
404 CO2(M)=BO2
405 CCO(M)=BCO
406 CCO2(M)=BCO2
407 CI(M)=BI
408 QR=0.0
409 GO TO 470
410 B20=(32.0*BO2)+(28.0*BCO)+(44.0*BCO2)+(A12*BI)
411 B21=B1/BTG
412 B22=(0.00000018*BTG)-0.000014
413 B23=(0.00000016*BTG)-0.00001
414 B24=(BCO2*B22)+((1.0-BCO2)*B23)
415 B25=10.57+(.0021*BTG)-(206000.0/(BTG*BTG))
416 B26=7.2+(.00086*BTG
417 B27=((BCO2*B25)+((1.0-BCO2)*B26))/B20
418 B28=(0.00000572*(BTG**1.82))/A7
419 B29=0.00013+(0.000000*BTG)
420 B30=BF/B2
421 B31=B30*B21*B20
422 B32=1.90*B31/B29
423 B33=B29/(B21*B20*B28)
424 B34=B27*B29/B24
425 B35=(515.0*R(M)*BTG*A19)/(EXPF(A20/TO(M)))
426 B36=7.73*B31/(B20*B21*(B32**0.45)*(B33**0.667))
427 B37=5.9*B27*B31/((B32**0.34)*(B33**0.667))
428 B38=3.45*B24*(B32**0.5)*(B33**0.5)
429 B39=(A5+(A6*0.90*(1.0-(R(M)*R(M))))*(1.0-BCO2-BI)*B21
430 840=(B35*B36*BO2*B21)/(B35+B36)
431 IF(0.999-R(M))432,441,441
432 RO2=B36*BO2*B21
433 RCO=B39*BO2*B21
434 IF(RCO)435,436,436
435 RCO=0.0
436 RC=RO2-RCO
437 IF((0.5*RO2)-RCO)438,440,440
438 RCO=0.5*RO2
```

Fig. 7.2 (continued)

```
439 RC=RCO
440 GO TO 447
441 B41*0.54*B28/(LOGF(1.0/R(M)))
442 IF(B41-B39)443,444,444
443 B39=B41
444 B42=(B36*B02)/(B41+B39+B36)
445 RC=B41*B42*B21
446 RCO=B39*B42*B21
447 RO=RC+RCO
448 IF(RO-B40)452,452,449
449 RO=B40
450 RC=0.5*B40
451 RCO=RC
452 R(M)=R(M)-(RC*B4/R(M))
453 B43=(RC-RCO)*A1*A4/B21
454 B44=BF+B43
455 B45=BF*B21
456 B46=B44*B21
457 CO2(M)=((BO2*B45)-(A4*RO*A1))/B46
458 IF(CO2(M))459,460,460
459 CO2(M)=0.0
460 CCO(M)=((BCO*B45)+(A4*2.0*(RC-RCO)*A1))/B46
461 IF(CCO(M))462,463,463
462 CCO(M)=0.0
463 CCO2(M)=((BCO2*B45)+(2.0*A4*RCO*A1))/B46
464 IF(CCO2(M))465,466,466
465 CCO2(M)=0.0
466 CI(M)=1.0-CO2(M)-CCO(M)-CCO2(M)
467 IF(CI(M))468,469,469
468 CI(M)=0.0
469 QR=((RC*136000.0)+(RCO*46000.0))*A4
470 B50=B37+B5
471 B51=B50*A4
472 B52=(A17*B7)+(B37*A4*BTG)+(B5*A4*TO(M))+QR
473 TOO=TO(M)
500 DO549KK=1,20
501 B53=((A17*(TOO**4.0))+(B51*TOO)-B52)/((4.0*A17*(TOO**3.0))+B51)
502 B54=ABSF(B53)
503 TOO=TOO-B53
504 IF(TOO)477,477,505
505 IF(B54-(.001*TOO))475,475,549
549 CONTINUE
474 GO TO 477
475 B55=(A18*(TOO**4.0))+(B37*BTG)+(B5*TC(M))+(QR/A4)
476 TCC=TC(M)
550 DO556KL=1,20
551 B56=((A18*(TCC**4.0))+(B50*TCC)-B55)/((4.0*A18*(TCC**3.0))+B50)
552 B57=ABSF(B56)
```

Fig. 7.2 (continued)

```
  553 TCC=TCC-B56
  554 IF(TCC)477,477,555
  555 IF(B57-(.001*TCC))479,479,556
  556 CONTINUE
  477 WRITE OUTPUT TAPE 9,1077,M,TOO,B53,TCC,B56
 1077 FORMAT (29HO NO SOLUTION FOR TEMPERATURE/5HO  M=I4,5H  TO=F10.4,6H
     1 DTO=E10.4,5H  TC=F10.4,6H  DTC=E10.4)
  478 GO TO 600
  479 B58=((A4*B37*(TOO-BTG))-(B38*(BTG-A16)))*A1/(B44*B21*B27*B20)
  480 IG(M)=BIG+B58
  481 QW(M)=((B38*(BTG-A16)))+(A17*((TOO**4.0)-B7)))/B3
  482 TO(M)=TOO
  483 TC(M)=TCC
  484 BO2=CO2(M)
  485 BCO=CCO(M)
  486 BCO2=CCO2(M)
  487 BI=CI(M)
  488 BF=B44*TG(M)/BTG
  489 BTG=TG(M)
  499 CONTINUE
  307 IF(CO2(M)-(.999*A8))399,399,308
  308 GO TO 600
  399 CONTINUE
  201 TI=K1
  202 TN3=N2
  203 TIME=(A2*TN3*TI)/60.0
  204 WRITE OUTPUT TAPE 9,1204,TIME
 1204 FORMAT(64HO                                    VERTICAL BED PROFILE
     1AT TIME=F10.2,8H MINUTES/70HO     BED
      2                          OUTSIDE,37H                              WA
      3LL HEAT/59H  POSITION     O2 MOLE     CO MOLE    CO2 MOLE   INERT
      4MOLE,59H   ROD TEMP   CENTER ROD   GAS TEMP      FLUX     INTERFAC
      5E/59H      CM        FRACTION    FRACTION    FRACTION   FRACTION  ,5
      68H   DEG K     TEMP DEG K    DEG K    CAL/CM2-SEC   FRACTION/1HO)
  205 DO249M=1,N1
  206 WRITE OUTPUT TAPE 9,1206,HT(M),CO2(M),CCO(M),CCO2(M),CI(M),TO(M),I
     1C(M),TG(M),QW(M),R(M)
 1206 FORMAT(F9.4,4F12.4,F14.2,3F12.1,F10.4)
  249 CONTINUE
  299 CONTINUE
  600 CALL EXIT
      END(1,1,0,0,0,0,0,0,0,0,0,0,0,0,0)
```

Fig. 7.2 (continued)

TEMPERATURE AND GAS COMPOSITION PROFILES

COMPUTER CODE NUMBER 500

INPUT DATA

HEIGHT INCREMENT (A1)	= 0.2000E-00	TIME INCREMENT (A2)	= 0.5000E 01
REACTOR RADIUS (A3)	= 0.6350E 01	NUMBER OF RODS (A4)	= 0.2900E 02
CO RATE CONST KI (AS)	= 0.6800E 07	CO RATE CONST K2 (A6)	= 0.5050E 06
PRESSURE (A7)	= 0.1360E 01	INITIAL O2 FR (AB)	= 0.1000E 01
INITIAL CO FR (A9)	= 0.	INITIAL CO2 FR (A10)	= 0.
INITIAL INERT FR (ALL)	= 0.	INERT MOL WT (A12)	= 0.
INITIAL FLOWRATE (A13)	= 0.1000E 01	INITIAL GAS TEMP (A14)	= 0.7730E 03
INITIAL WALL TEMP(A15)	= 0.9730E 03	WALL TEMP (A16)	= 0.9730E 03
RAD CONSTANT KO (A17)	= 0.3450E-10	RAD CONSTANT KC (A18)	= 0.1270E-11
KIN CONSTANT A (A19)	= 0.2000E 05	KIN CONSTANT E/R (A20)	= 0.1070E 05
INTERFACE FR (A21)	= 0.1000E 01	NO OF HT INCR (N1)	= 100
TIME INC PER PR (N2)	= 12	PRINT OUT PER RUN (N3)	= 3

VERTICAL BED PROFILE AT TIMES = 1.00 MINUTES

BED POSITION CM	O2 MOLE FRACTION	CO MOLE FRACTION	CO2 MOLE FRACTION	INERT MOLE FRACTION	OUTSIDE ROD TEMP DEG K	CENTER ROD TEMP DEG K	GAS TEMP DEG K	WALL HEAT FLUX CAL/CM2-SEC	INTERFACE FRACTION
0.2000	0.9560	0.	0.0440	0.0000	1858.04	2064.4	918.4	9.5	0.9575
0.4000	0.9089	0.	0.0911	0.0000	1883.07	2091.6	1061.0	10.1	0.9566
0.6000	0.8595	0.	0.1405	0.0000	1900.41	2108.5	1195.8	10.5	0.9562
0.8000	0.8086	0.	0.1914	0.0000	1909.38	2114.6	1318.5	10.7	0.9561
1.0000	0.7568	0.	0.2432	0.0000	1911.71	2112.2	1426.4	10.8	0.9567
1.2000	0.7048	0.	0.2952	0.0000	1906.88	2100.8	1517.9	10.7	0.9576
1.4000	0.6535	0.	0.3465	0.0000	1895.22	2081.0	1592.3	10.4	0.9587
1.6000	0.6034	0.	0.3966	0.0000	1877.54	2054.2	1649.9	10.0	0.9598
1.8000	0.5552	0.0032	0.4416	0.0000	1855.34	2022.1	1691.9	9.5	0.9610
2.0000	0.5090	0.0143	0.4767	0.0000	1829.86	1986.2	1720.0	9.0	0.9625

Fig. 7.3. Output Format from the Computer Solution of the Mathematical Model.

reaction temperature is high enough to ensure that the first-order kinetics does not contribute to reaction control, then, at the beginning of a differential element test, the reaction rate of oxygen and graphite depends only upon the mass transfer across the external film.

Equation (3.8) can be rearranged to give:

$$k_g = \frac{R}{2\pi r_E (C_{O_2} - C_{O_2}^E)} . \tag{8.1}$$

Since the rate of reaction at the reaction site is very rapid and does not contribute to reaction control, the oxygen concentration at the exterior surface of the differential element, $C_{O_2}^E$, will be zero. Equation (8.1) will then reduce to:

$$k_g = \frac{R}{2\pi r_E C_{O_2}} . \tag{8.2}$$

The external mass transfer coefficient can be determined from Eq. (8.2) with the over-all oxygen reaction rate, R, the radius of the fuel rod r_E, and the bulk gas oxygen concentration C_{O_2}. This mass-transport coefficient is usually dependent on the Reynolds number, therefore the Reynolds number would have to be varied to establish a usable correlation.

8.2 Rate Constants for the Oxidation of Carbon Monoxide

During the initial part of the reaction, when the reaction interface is close to the surface of the differential fuel element, the reaction of oxygen with CO will be dependent on the available fuel rod external surface, which can be represented by the constant k_{c_1} in Eq. (6.11).

For tests with high Reynolds numbers, external mass transport does not contribute to reaction control so the oxygen concentration at the exterior surface of the fuel element will be equal to the oxygen

concentration in the bulk gas-phase. If only the initial reaction rate is considered ($r_E = r_I$) and for pure oxygen as the oxidizing gas,

$$C^E_{O_2} = C^I_{CO} = C_{O_2} \ .$$

This can be applied to Eq. (6.11) to give:

$$R_{CO} = k_{c_1} \, (C^E_{O_2})^2 \ . \tag{8.3}$$

Upon rearranging this gives an equation defining the external surface rate constant k_{c_1}:

$$k_{c_1} = \frac{R_{CO}}{(C_{O_2})^2} \ . \tag{8.4}$$

Equation (8.4) can be used to determine k_{c_1} if the initial reaction rate of the CO-oxygen reaction is known at a known bulk gas-phase oxygen concentration.

After the reaction has progressed for a while the external surface of the differential element will be much different from the position of the reaction interface because of the reaction ash buildup. This will allow determination of the second rate constant for the O_2-CO reaction k_{c_2}. Equation (8.4) can be substituted into Eq. (6.11), and after rearrangement this gives:

$$k_{c_2} = \frac{\dfrac{R_{CO}}{(C_{O_2})^2} - k_{c_1}}{(r_E^2 - r_I^2)} \ . \tag{8.5}$$

Thus, knowledge of the CO-oxygen reaction rate R_{CO} (CO_2 production rate) and the position of the reaction interface position r_I (obtained from material balance relationships) allows determination of the two rate constants for oxidation of CO, k_{c_1} and k_{c_2}.

8.3 Internal Mass-Transport Property

The internal mass transport property αD can be determined by establishing the O_2-C reaction rate for high Reynolds number after r_E is different from r_I and rearranging Eq. (3.14) with substitution of Eq. (8.3):

$$\alpha D = \frac{R_C \ln \frac{r_E}{r_I}}{4\pi C_{O_2}} . \tag{8.6}$$

A continuous record of the O_2-C reaction rate and the O_2-CO reaction rate for different element tests at known conditions of gas composition, temperature, and flow rate will allow determination of the rate constants and mass transport properties of interest.

8.4 Experimental

A crude experimental setup for the differential element tests was made in order to get a rough approximation of the constants of interest. A thermogravimetric balance with provisions for gas preheating and off-gas sampling was used. This setup allows suspension of a segment of a fuel rod by means of a platinum weighing basket into a heated zone into which a heated, oxygen-bearing gas was introduced (Fig. 8.1). The off-gas was monitored for CO and CO_2 content by a gas-adsorption chromatograph. The change in element weight allowed determination of the oxygen-graphite reaction rate R_C, and the CO and CO_2 content in the off-gas allowed determination of the O_2-CO reaction rate constants.

Results from one such differential bed test are presented in Appendix 14.4. For more precise values of the constants of interest and particularly for temperature effects on these constants, an enlarged experimental program would be necessary.

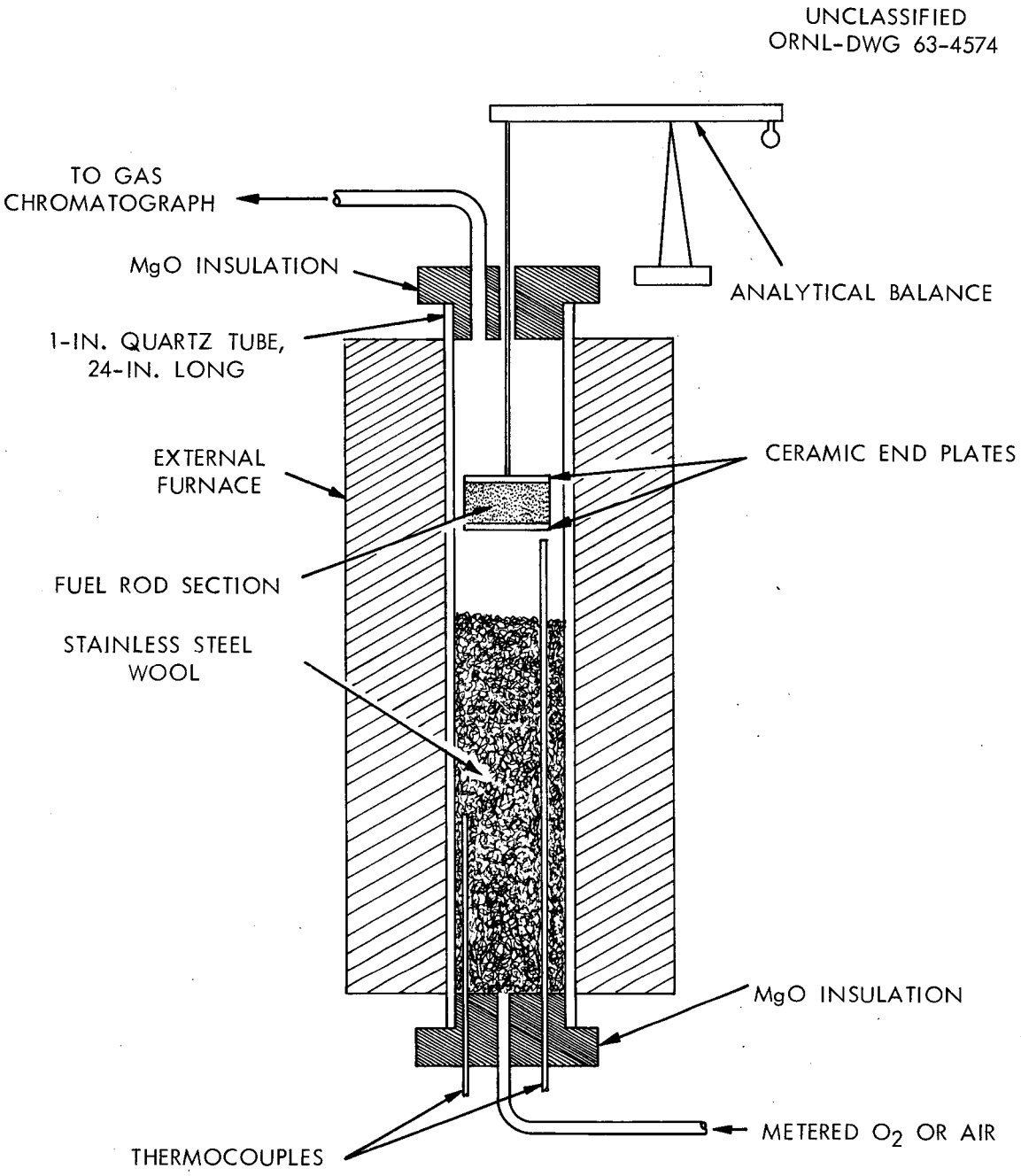

Fig. 8.1. Experimental Setup for Differential Fuel Rod Section Tests.

9. COMPARISON BETWEEN PREDICTED AND EXPERIMENTAL RESULTS

The end result of the mathematical analysis of the fixed-bed oxidation of graphite-uranium fuel by oxygen-bearing gas is to be able to predict system gas composition and temperature as a function of bed position, reaction time and operating conditions. If these results approximate actual operating results, then the mathematical analysis can be used with some assurance to predict results with a variety of operating conditions, and it could be the basis of correlation of experimental data. It will also be useful in pointing out areas of potential operational problems that could then be further investigated experimentally.

In some of the early experimental tests on the fixed-bed oxidation of Kiwi-type fuel rods there are good records of the effluent gas composition as a function of operating conditions and in two tests the system temperature was measured for a considerable period of the test.[3,15] The majority of the experimental information on the systems is with a 2-1/2-in.-diam oxidation vessel in which various operating conditions were varied, and in one test with a 5-in.-diam reactor.

9.1 Two-and-one-half-inch-diameter Reactor

In test 0-1, five Kiwi-type fuel rods 8-1/3-in. long were used in the fixed bed in a 2-1/2-in.-diam reactor, and an O_2-Ar mixture was used as the oxidizing gas.[3] The O_2-Ar feed was changed in rate and oxygen content at intervals during the test, and the effluent off-gas and internal temperatures were periodically measured. This system was approximated with the computer code by considering each set of constant operating conditions as a separate case, and, when a step change in feed gas rate or composition occurred, average bed conditions were used as the beginning of a new case.

It was found that the experimental values of effluent gas composition and system temperature were approximated fairly well by the mathematical model (Figs. 9.1 and 9.2). Predicted system temperatures were somewhat lower than the measured values during the latter part of the test and the effluent gas composition was predicted somewhat higher than the experimental measurement immediately after one of the step changes in feed gas composition and flow rate.

In tests 0-3 and 0-5 (ref 3), the experimental setup was similar to test 0-1, but experimental conditions were maintained fairly constant for the initial part of the tests. The predicted effluent compositions (only measured value) were within acceptable limits (Figs. 9.3 and 9.4).

9.2 Five-inch-diameter Reactor

In the only test made with a short 5-in.-diam reactor (run 0-12) containing 29 short Kiwi-type fuel rods,[16] although experimental conditions were changed several times during the test, predicted results were fairly close to experimental results (Figs. 9.5 and 9.6). This is probably because experimental conditions for the 5-in.-diam reactor were fairly close to the assumed model of the system.

9.3 Utility of Mathematical Analyses

Since the mathematical model apparently is capable of predicting gas composition and system temperatures to a fair degree of accuracy, use of these predictions for optimizing operating conditions seems reasonable if the Kiwi-B-1B-type fuel rod is used.

10. PREDICTIONS FOR LARGE-SCALE REACTORS

It is generally considered that the maximum size of a tubular reactor for oxidation of Kiwi-type fuel rods in a fixed bed will be 5 in. in

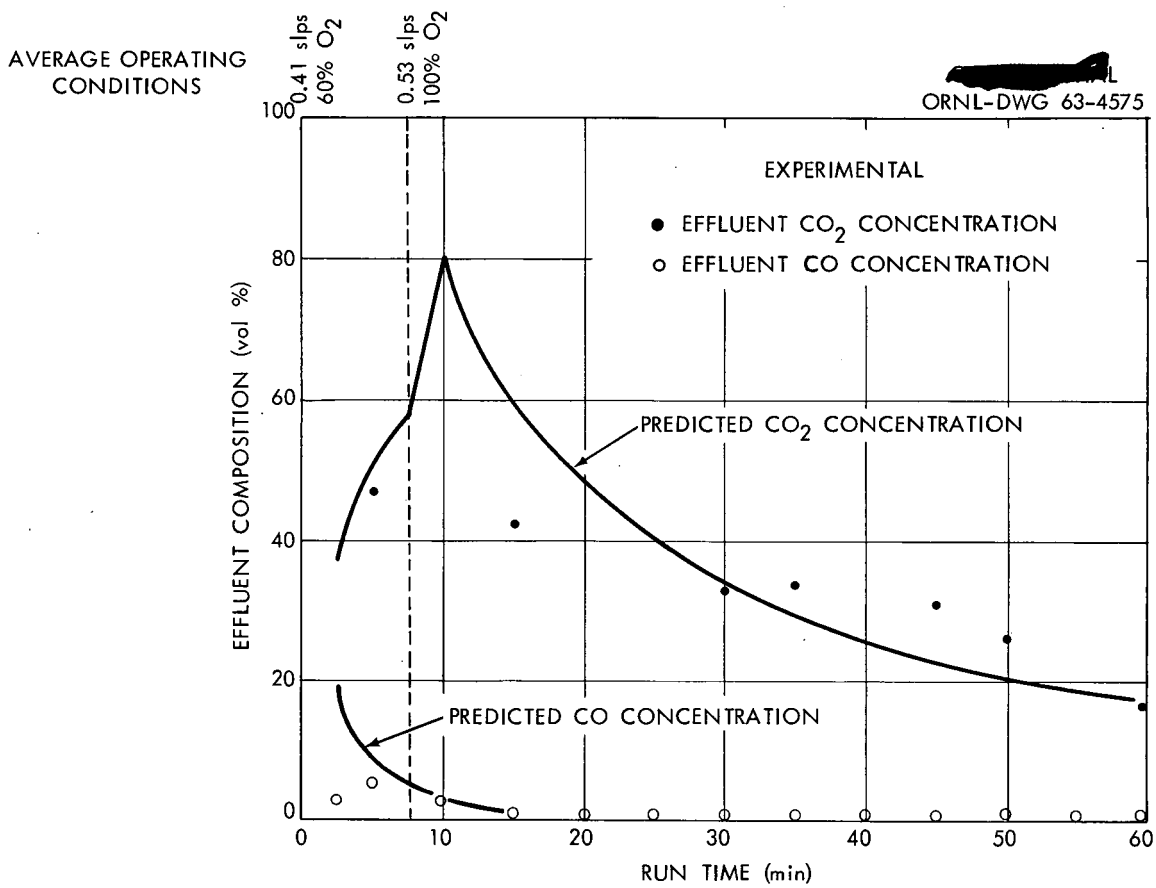

Fig. 9.1. Effluent Gas Composition Comparison Between Model-Predicted Results and Experimental Results for Run 0-1 Made with a 2-1/2-in.-diam Reactor Containing 5 Fuel Rods 8-1/3 in. Long.

[redacted]

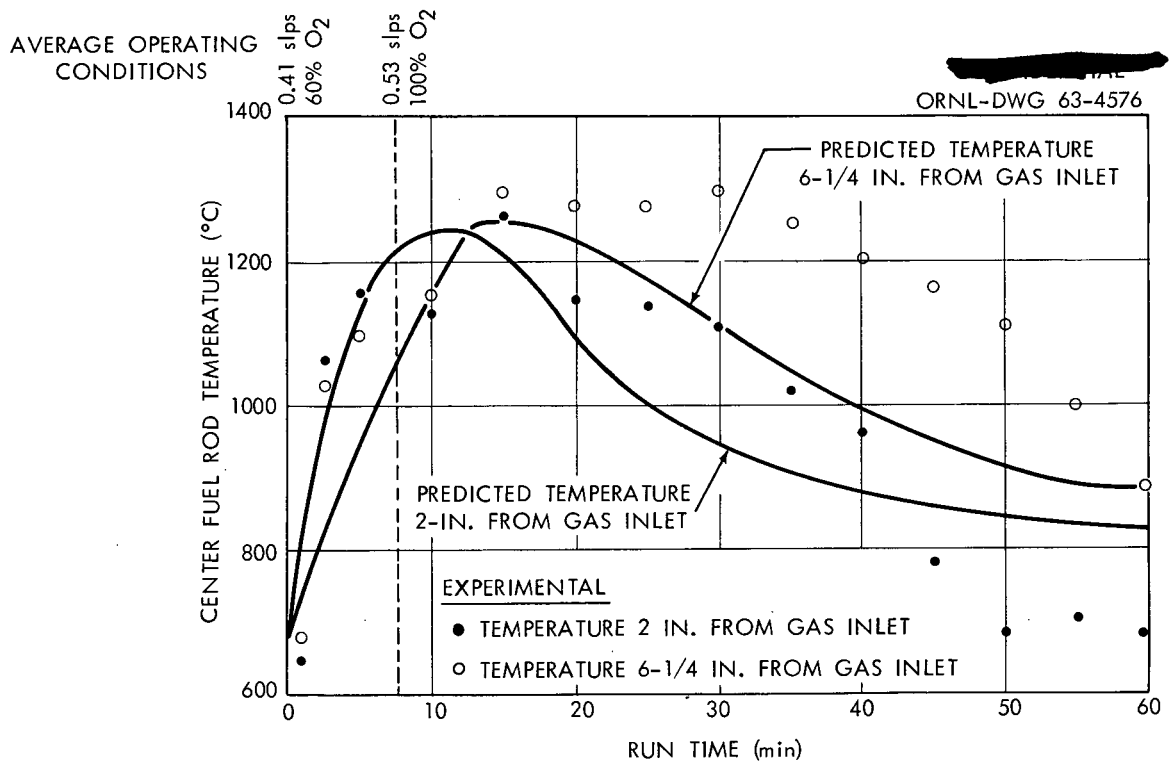

Fig. 9.2. Center-Line Temperature Comparison Between Model-Predicted Results and Experimental Results for Run 1 Made with a 2-1/2-in.-diam Reactor Containing Five Fuel Rods 8-1/3 in. Long.

[redacted]

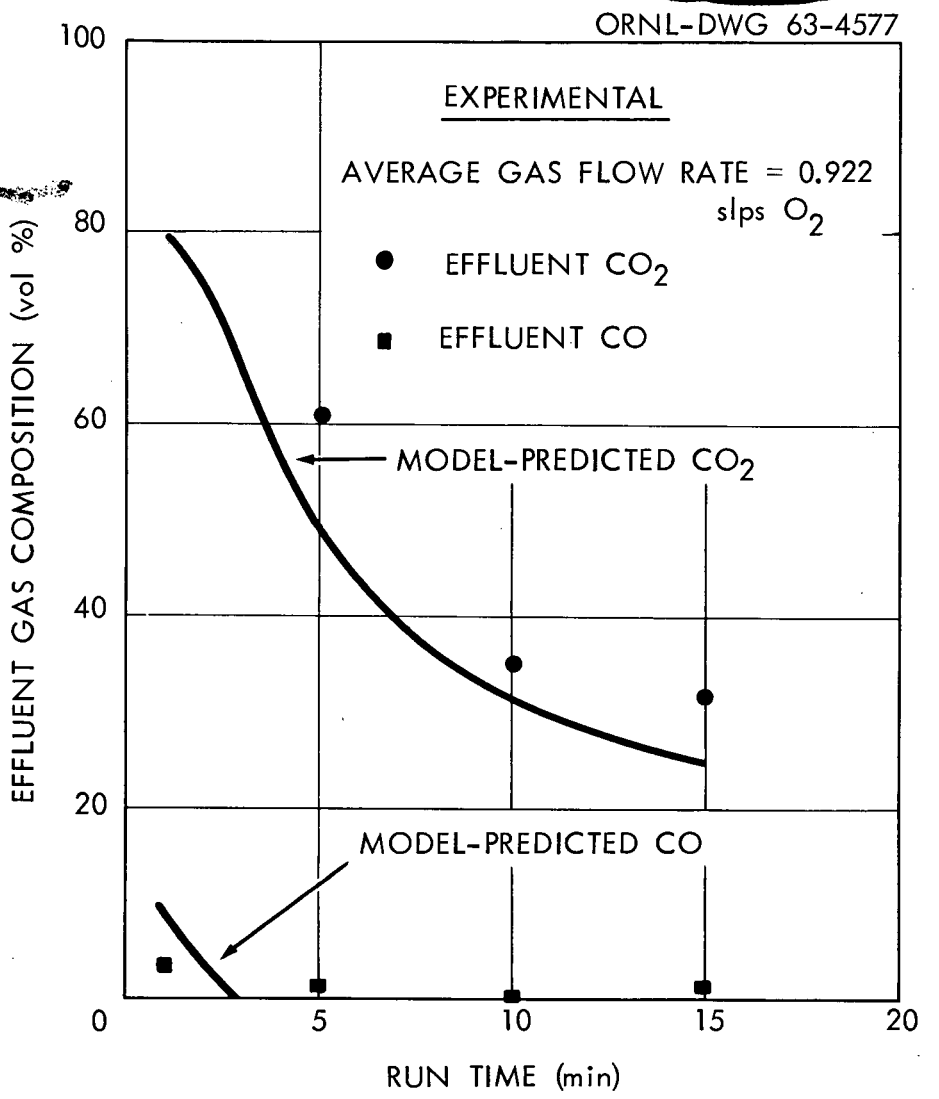

Fig. 9.3. Effluent Gas Composition Comparison Between Model-Predicted Results and Experimental Results for Run 0-3 Made with a 2-1/2-in.-diam Reactor Containing Five Fuel Rods 8-1/3 in. Long.

[redacted]

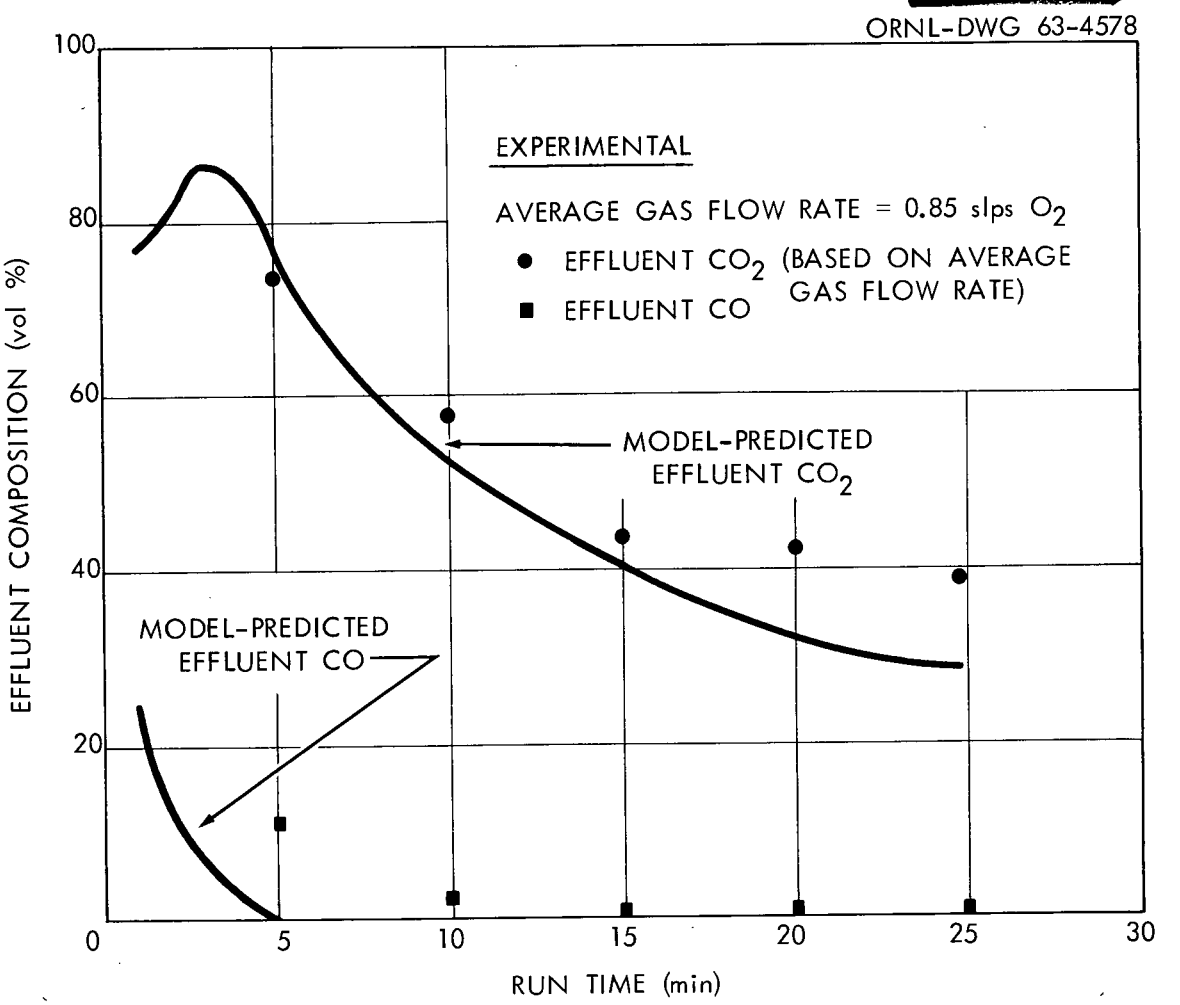

Fig. 9.4. Effluent Gas Composition Comparison Between Model-Predicted Results and Experimental Results for Run 0-5 Made with a 2-1/2-in.-diam Reactor Containing Five Fuel Rods 8-1/3 in. Long.

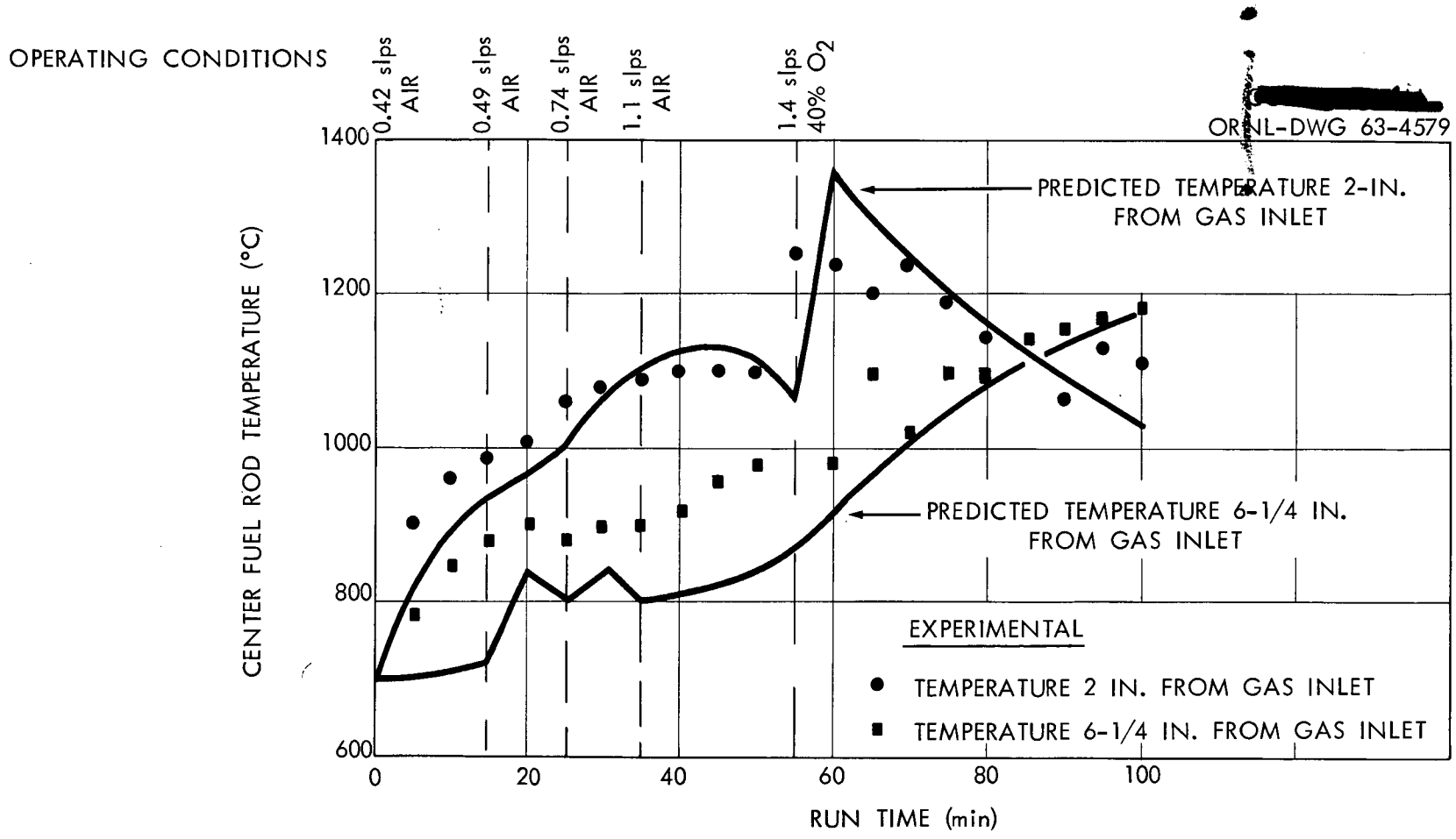

Fig. 9.5. Center-Line Temperature Comparison Between Model-Predicted Results and Experimental Results for Run 0-12 Made with a 5-in.-diam Reactor Containing 29 Fuel Rods 12-1/2 in. Long.

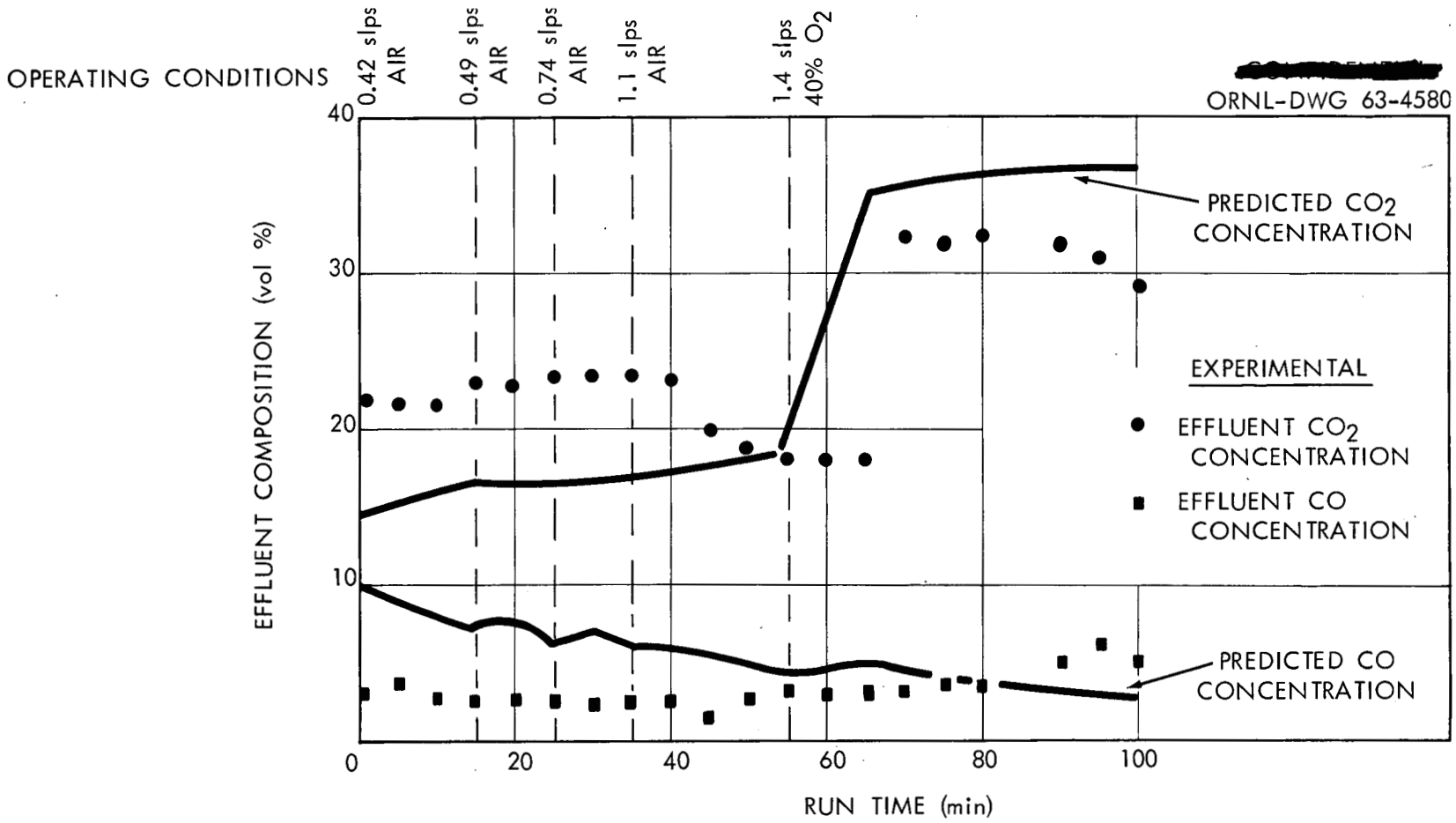

Fig. 9.6. Effluent Gas Composition Comparison Between Model-Predicted Results and Experimental Results for Run 0-12 Made with a 5-in.-diam Reactor Containing 29 Fuel Rods 12-1/2 in. Long.

diameter.[17] This restriction is mainly due to criticality considerations. Another possibility for a large-scale reactor is use of "slab-geometry" in which a 2-1/2-in.-thick rectangular reactor of indefinite width would be used.

The mathematical model will be usable in predicting conditions for the 5-in.-diam reactor, and it can be used to approximate the 2-1/2-in. slab (by use of a 2-1/2-in.-diam reactor). The latter will give results that will approach results from a 2-1/2-in. x 2-1/2-in. rectangular reactor but will just give the lower limit for an extended width. Use of broken fuel rods instead of whole rods may change the results since there is no assurance that the bed will maintain its shape during the burning operation. This analysis may not be usable for other types of fuel in which the oxidation ash does not sinter to the fuel; however, a similar analysis could be made for that case.

10.1 Potential Problems

Two major problems are expected for large-scale reactors. These are: (1) potential explosive gas mixtures in the reactor effluent (more than 12.5% CO) and (2) excessive temperatures in the fixed bed. Initial experimental results indicate that if the ash temperature is allowed to exceed 1350°C for extended periods, some ash melting will result.[15,16] This is detrimental because fluorination of the molten ash for uranium recovery is difficult. In order to prevent gross ash melting, the requirement that the maximum reactor temperature must not exceed 1350°C has been established.[16,17]

The problem of the CO content of the effluent can be solved in two ways. These are: (1) always maintain the CO content in the reactor at less than 12.5% and (2) make provisions for gas dilution by an inert gas

at the reactor effluent. In either case it is necessary to be able to predict the effluent gas composition. The most desirable operating procedure would be to always maintain the CO concentration at less than 12.5% at all points in the reactor.

A further restriction is that the linear gas velocity in the reactor at the point where the gas leaves the reactor should not exceed 3 fps.[14,15] If this velocity is exceeded, there is a problem of ash removal from the reactor proper by attrition and fluidization. Obviously the reactor wall heat flux should not be excessive. A maximum value of about 7.5 cal cm^{-2} sec^{-1} is acceptable.[14,15]

10.2 Five-inch-diameter Reactor

A series of solutions of the mathematical model was made for the 5-in.-diam reactor by the computer code. A total of 29 Kiwi-type fuel rods were assumed to be vertically arrayed in the reactor with a maximum length of 100 cm. The following range of operating conditions was investigated:

Gas flow rate: 0.1 to 100 slps

Feed gas composition: 21 to 100% oxygen (remainder nitrogen)

Initial ash build-up: 0 to 5%

Increasing the gas flow rate had two major effects on the maximum reactor temperature: (1) increasing the reaction rate and thus heat generation and; (2) increasing the amount of convective heat transfer. This resulted in an increase of maximum system temperature when the gas flow rate was initially increased but a decrease in maximum gas temperature at the very high flow rates (100 slps) because of the additional convective heat transfer (Fig. 10.1).

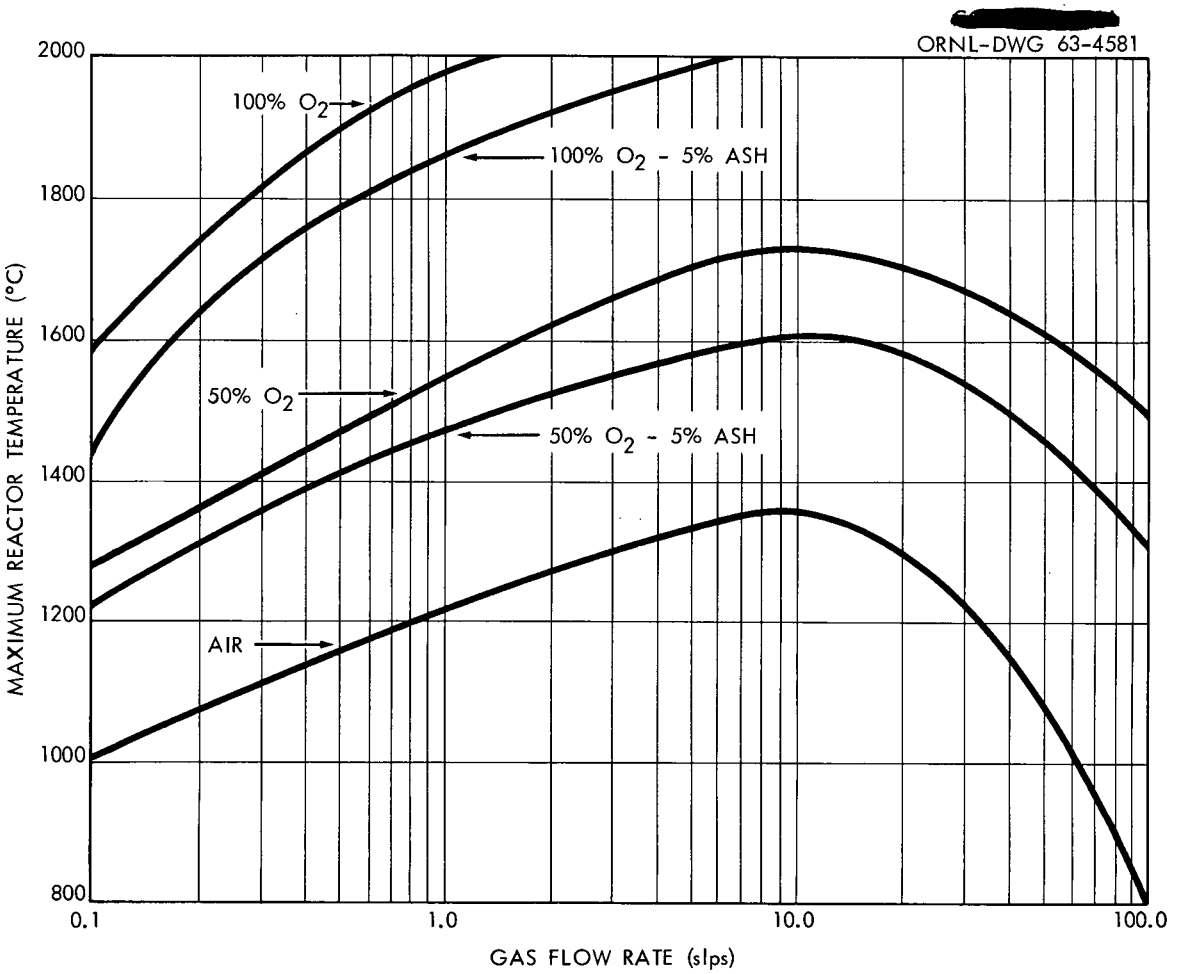

Fig. 10.1. Predicted Maximum Reactor Temperature as a Function of Feed Gas Composition and Flow Rate for the 5-in.-diam Reactor with 29 Fuel Rods.

Decreasing the initial oxygen concentration to 50% (with 50% nitrogen) resulted in over-all lowering of the maximum temperature, with the same general effects of gas flow rate. A further reduction of the oxygen content of the inlet gas to that of air resulted in a further reduction of maximum temperature, and, at high gas flow rates, the reaction was not even sustained (reaction temperature was less than wall temperatures).

When an ash layer was allowed to build up on the fuel rod prior to the actual oxidation step, the maximum gas temperature was further lowered, with similar effects from change in gas flow rate (Fig. 10.1). In this case, the reaction rate was retarded due to resistance of the ash layer. The fuel can be "pre-ashed" by allowing oxygen or air to flow into the reactor during the reactor heating-up period. (It is estimated that up to 5% of the fuel volume can be oxidized to ash in this manner.)[16]

Maximum CO content of the gas was also affected by change in gas flow rate, oxygen content of feed gas, and presence of fuel ash. The change in maximum CO content was small for change in gas flow rate; however, the addition of a diluent and the presence of fuel ash decreased the CO content (Fig. 10.2). The diluent acted in two ways: (1) dilution effect in which CO was replaced with an inert, and (2) lowered temperature of oxidation which was more conducive to CO_2 formation. Presence of the fuel ash reduced the CO content because it gave more surface area for the O_2-CO reaction as well as a reduction in the reaction temperature.

The heat flux at the reactor wall was also found to be dependent on gas flow rate (increasing with gas flow rate and finally decreasing with very high gas flow rate), oxygen content of inlet gas (decreased with oxygen content), and presence of fuel ash (decreased with ash build-up)

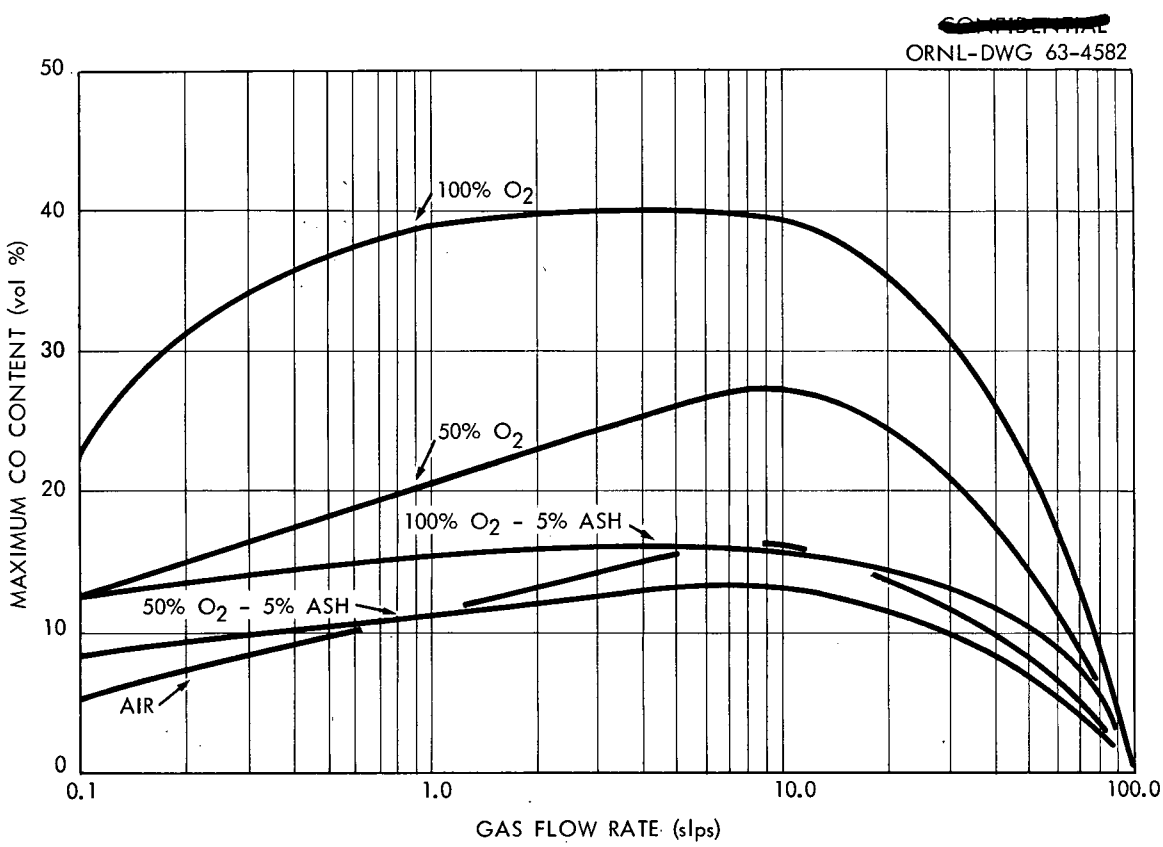

Fig. 10.2. Predicted Maximum Carbon Monoxide Content as a Function of Feed Gas Composition and Flow Rate for the 5-in.-diam Reactor with 29 Fuel Rods, 100 cm Long.

(see Fig. 10.3). The wall heat flux might be a limiting factor if it exceeds a value which is beyond design capability (about 7.5 cal cm^{-2} sec^{-1} or 100,000 Btu ft^{-2} hr^{-1}.

An interesting fact was discovered during this mathematical analysis. The oxidation occurred in a zone of bed height which could vary from about 2 to 100 cm (see Fig. 10.4). This zone of oxidation (defined as that portion of the bed in which the oxygen content of the bulk gas was higher than 1%) was affected by gas flow rate (increasing flow rate increased zone length), oxygen content (decreasing oxygen content increased zone length) and ash build-up (ash increased zone length) (see Fig. 10.4). The zone concept showed that, with relatively low gas flow rates (less than 10 slps), only a small portion of a fixed bed would be undergoing oxidation from a single gas inlet, at least during the early stages of the oxidation before gross ash build-up. Thus, to achieve maximum oxidation in a deep bed of fuel it would be desirable to have multiple gas inlets spaced at intervals up the length of the bed. If the multiple inlets were used, the first such zone would have the most severe conditions of reaction rate, temperature, CO content, and heat flux. The dilution effect of the CO_2 from the first zone would greatly influence subsequent zones.

10.2.1 Optimum Operating Conditions for 5-in.-diam Reactor

When determining optimum operating conditions for the 5-in.-diam reactor, it should be noted that the most severe conditions will exist in the early phases of the reaction. (Maximum temperature and CO content of most experimental tests occurred within 30 min of the start of reaction.) This may not be the case for fuel in which the ash does not adhere to the fuel. After this initial phase of operation, system control becomes much less of a problem, and changes in gas flow rates or oxygen content of

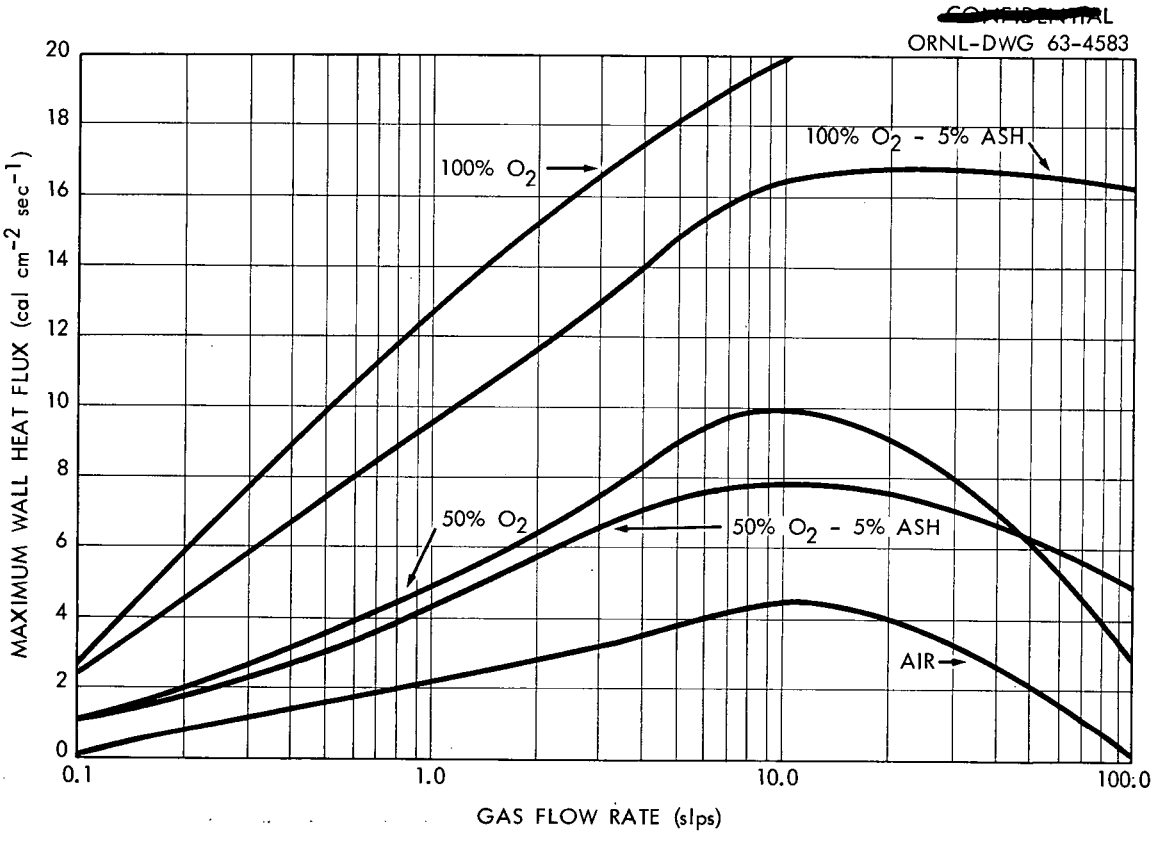

Fig. 10.3. Predicted Maximum Wall Heat Flux as a Function of Feed Gas Composition and Flow Rate for the 5-in.-diam Reactor with 29 Fuel Rods.

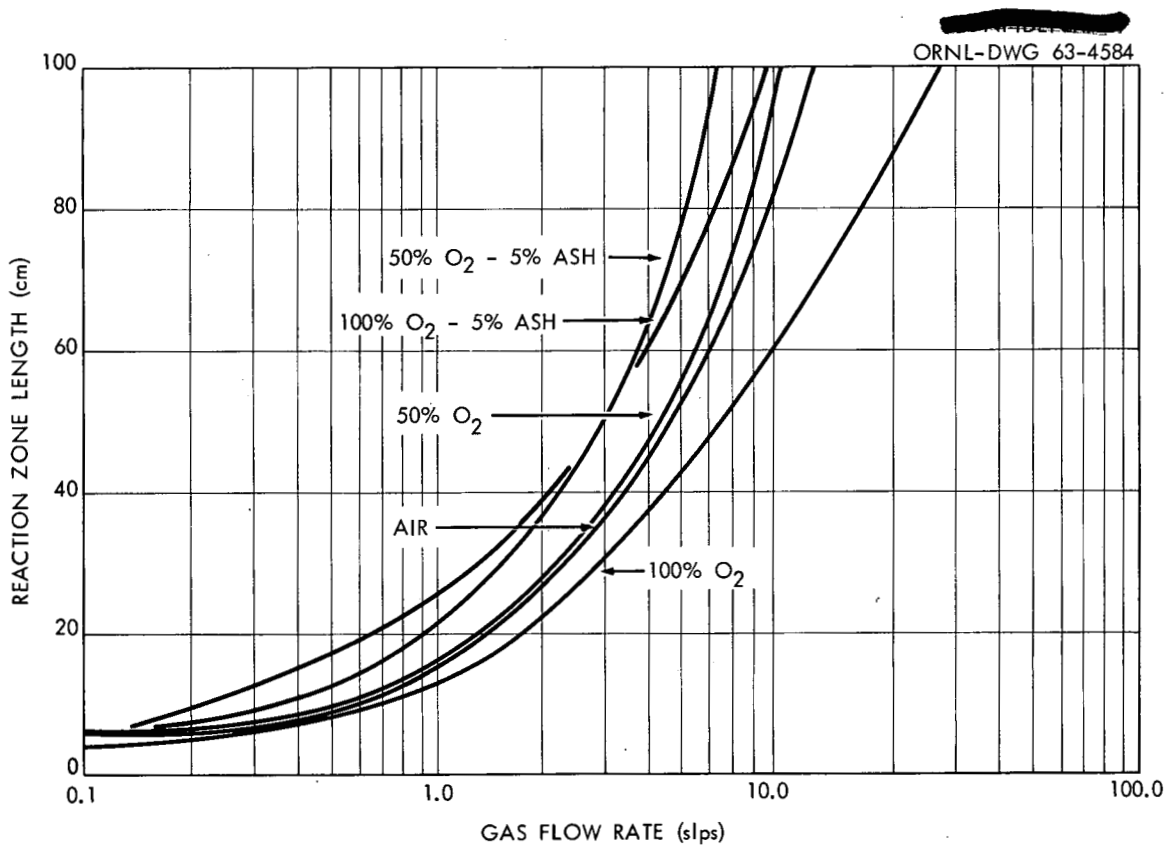

Fig. 10.4. Predicted Reaction Zone Length as a Function of Feed Gas Composition and Flow Rate for the 5-in.-diam Reactor with 29 Fuel Rods.

inlet gas would be made only in the interest of using the minimum amount of gas necessary.

Several different initial operating conditions for the 5-in. reactor in the first zone can be used for safe operation. The preceding plots involving temperature, CO content and heat flux can be used to establish safe operating conditions. One such set of initial operating conditions that can be used is 50% O_2—50% N_2, with 5% ash build-up, at a gas flow rate of 1.0 slps. Other zones in the reactor can be operated at safe conditions in a similar manner. For example, zone 2 could be run at 100% oxygen at 1.0 slps and 5% ash buildup since the effluent from zone one would act as the diluent. Or, if there is no ash buildup, use of air at 1.0 slps would be suitable for zone 1 and 50% O_2 at 1.0 slps for zone 2.

10.2.2 Length of Oxidation Cycle for 5-in.-diam Reactor

The length of the oxidation cycle for the 5-in.-diam reactor was determined from the computer solution of the mathematical model. This was done by predicting the amount of oxidation that occurred in one zone during a 30-min period of constant, safe, operating conditions, then readjusting the operating conditions for optimum, safe operation and allowing another 30 min of operation, etc. When more than 99% of the available graphite in one zone was exhausted, the oxidation cycle was considered to be finished. An oxidation cycle of 4 hr was found to be suitable for the 5-in.-diam reactor and the operating conditions are shown in Table 10.1.

10.3 Two-and-one-half-inch-diameter Reactor

The mathematical model was also used to predict results in a 2-1/2-in.-diam reactor in which seven Kiwi-type fuel rods were used. The

Table 10.1. Proposed Operating Conditions for the First Zone of a 2-1/2-in.-diam Reactor and a 5-in.-diam Reactor

Oxidation Time (hr)	Gas Feed Rate (slps)		O_2 Content of Feed Gas (%)		% Carbon Reacted	
	2-1/2-in.	5-in.	2-1/2-in.	5-in.	2-1/2-in.	5 in.
0	0.25	1.00	50	21	0	0
0.5	0.25	1.00	100	50	13.5	4.0
1.0	0.25	1.00	100	100	37.5	15.2
1.5	0.25	1.00	100	100	61.8	39.2
2.0	0.20	0.75	100	100	77.8	64.0
2.5	0.20	0.75	100	100	88.4	78.8
3.0	0.10	0.50	100	100	96.0	89.1
3.5	-	0.50	-	100	100	97.4
4.0		-		-		100.0

range of operating conditions investigated for this reactor were:

Gas flow rate: 0.01 to 10 slpm

Feed gas composition: 21 to 100% O_2

Initial ash build-up: 0 to 5%

Change of the operating variables had similar results as those shown in calculations for the 5-in.-diam reactor and for the same reasons (see Figs. 10.5, 10.6, and 10.7). The reaction was again found to be confined to a zone of about 2 to 100 cm (see Fig. 10.8), which would necessitate design of a multiple gas-inlet reactor for best results.

10.3.1 Optimum Operating Conditions for 2-1/2-in.-diam Reactor

Two safe initial operating conditions for the first zone of a 2-1/2-in. reactor are: (1) 50% oxygen at a mass flow rate of 0.1 slps or (2) 50% O_2 at a mass flow rate of 1.0 slps 5% ash.

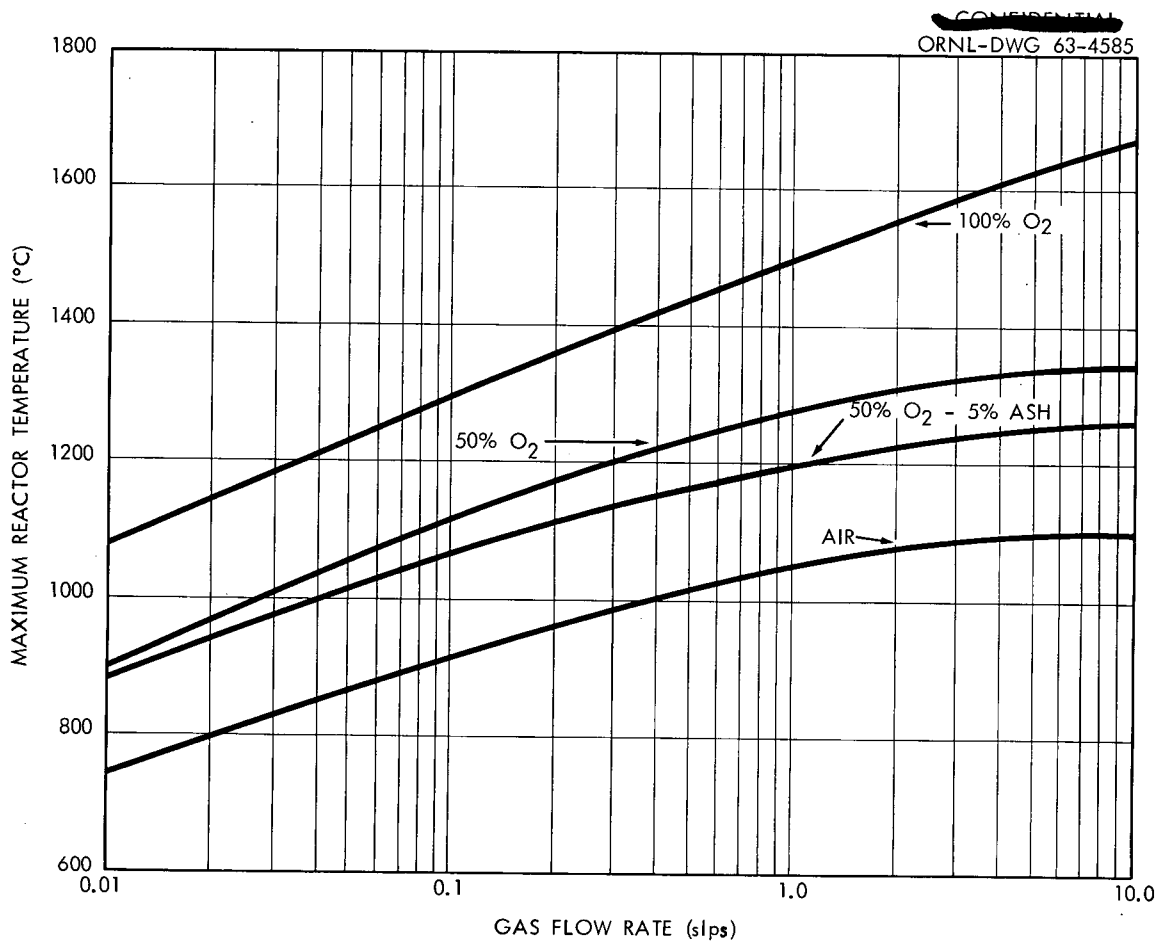

Fig. 10.5. Predicted Maximum Reactor Temperature as a Function of Feed Gas Composition and Flow Rate for the 2-1/2-in.-diam Reactor with Seven Fuel Rods.

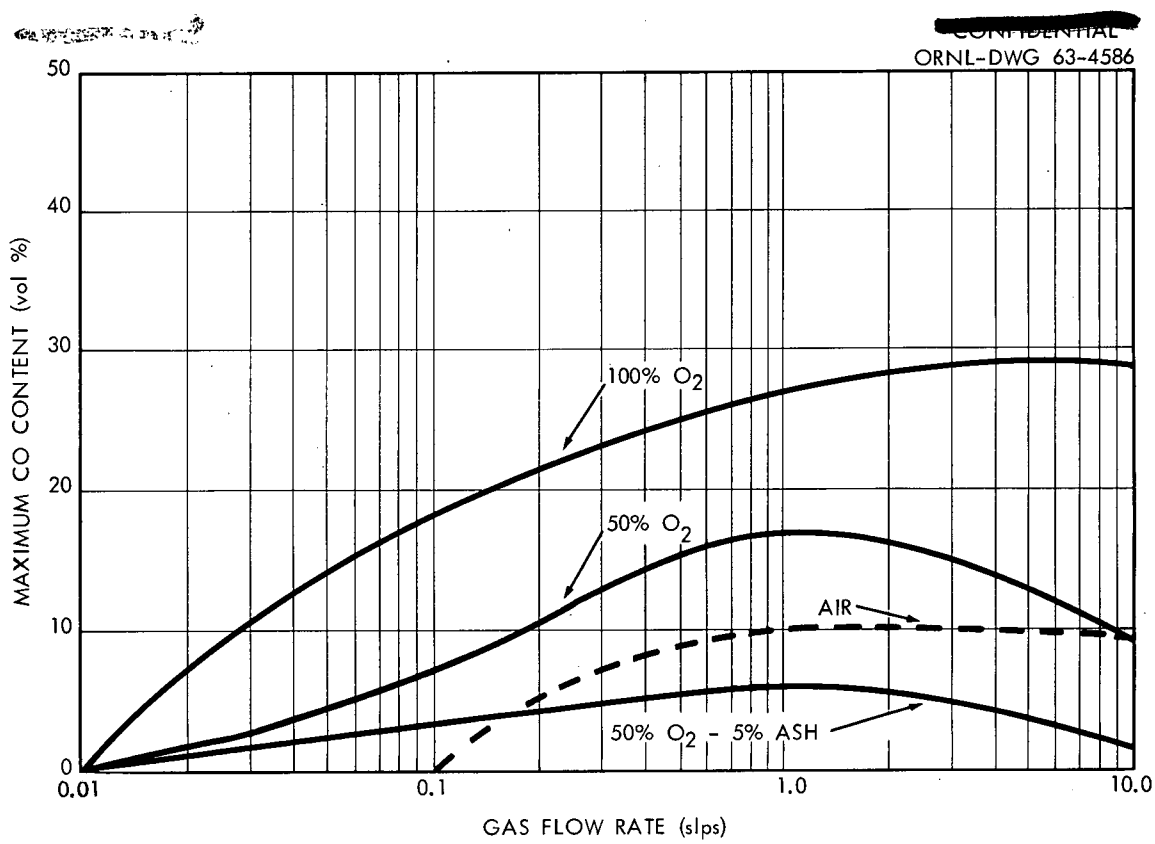

Fig. 10.6. Predicted Maximum Carbon Monoxide Content as a Function of Feed Gas Composition and Flow Rate for the 2-1/2-in.-diam Reactor with Seven Fuel Rods, 100 cm Long.

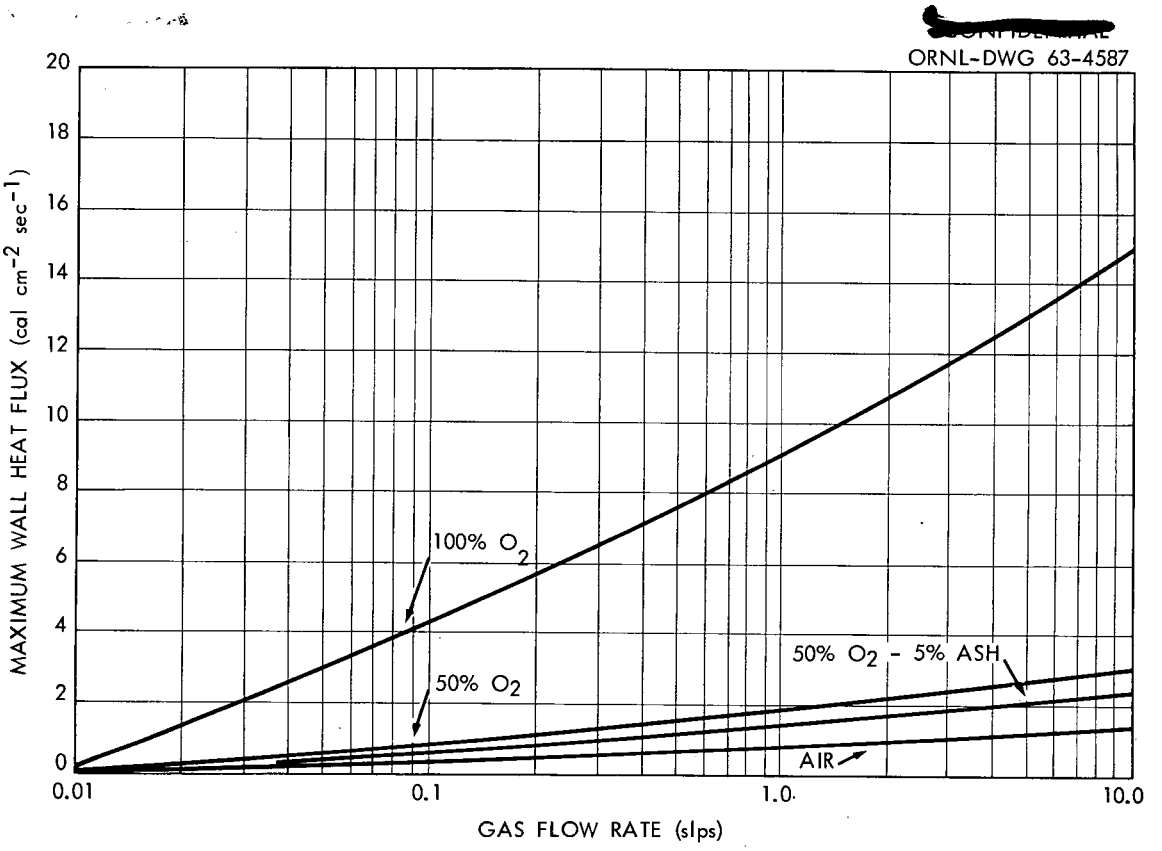

Fig. 10.7. Predicted Maximum Wall Heat Flux as a Function of Feed Gas Composition and Flow Rate for the 2-1/2-in.-diam Reactor with Seven Fuel Rods.

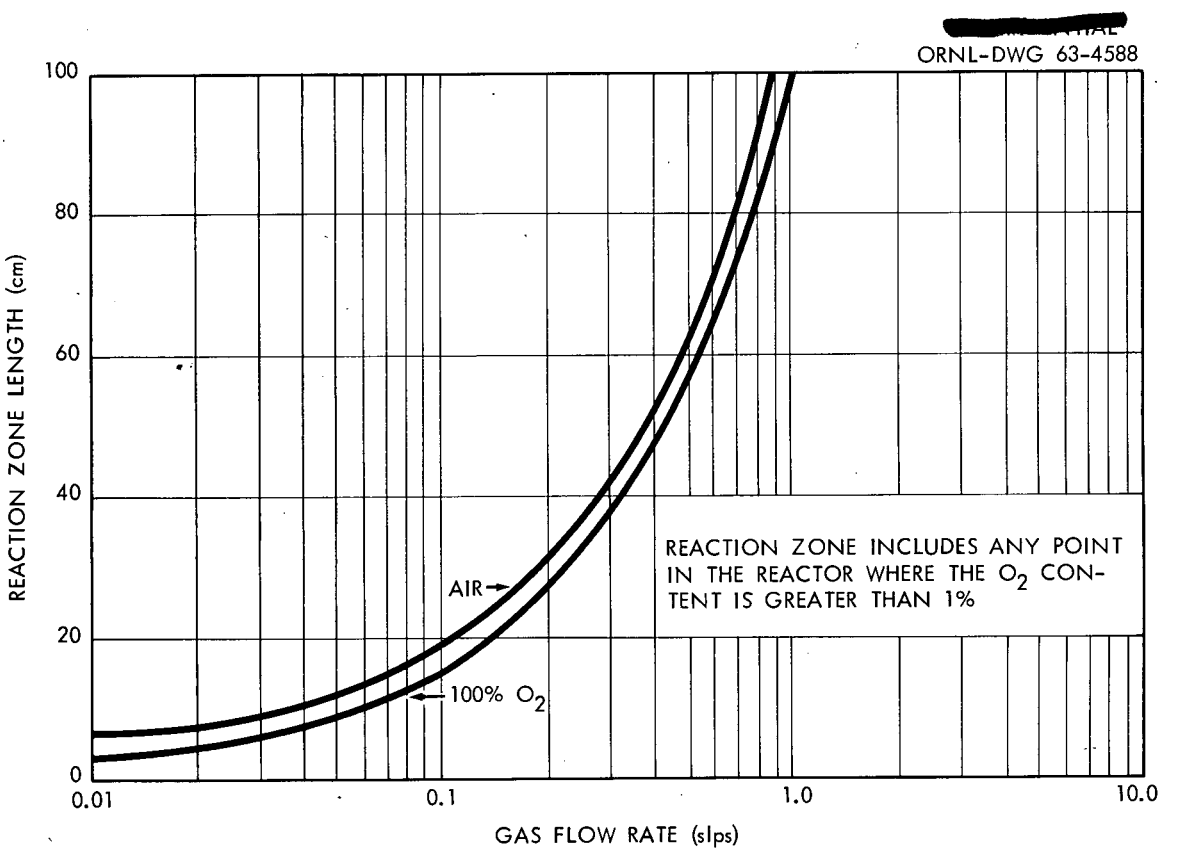

Fig. 10.8. Predicted Reaction Zone Length as a Function of Feed Gas Composition and Flow Rate for the 2-1/2-in.-diam Reactor with Seven Fuel Rods.

10.3.2 Length of Oxidation Cycle for 2-1/2-in.-diam Reactor

The length of the oxidation cycle for the 2-1/2-in.-diam reactor determined in the same manner as that for the 5-in.-diam reactor was 3-1/2 hr. Table 10.1 lists the operating conditions for this oxidation cycle.

11. CONCLUSIONS AND RECOMMENDATIONS

Mathematical analysis of the fixed-bed, graphite-uranium-fuel oxidation by an oxygen-bearing gas was shown to be an effective tool in predicting the behavior of large-scale reactors.

11.1 Conclusions

The results from the mathematical analysis can be used as a guide for the future experimental program as well as a means of predicting behavior in anticipated production-scale reactors and showing optimum, safe operating conditions. The results have specific application to Kiwi-B-1B-type fuel or other types which have simular properties.

According to the analysis, the major problems to be expected in this reaction system are: (1) excessive CO content of the gas; (2) excessive fuel-rod temperature, resulting in ash melting; and (3) excessive wall heat flux. The concept of zone oxidation or depletion of the oxygen content of the gas stream in a relatively small section of the fixed-bed was also shown to be an important factor. Changes in the gas flow rate, oxygen composition of inlet gas and oxidation ash build-up were shown to have the following effects on system behavior:

1. Gas flow rate: An increase in gas flow rate results in an increase in maximum system temperature, CO content, maximum wall heat flux, and length of oxidation zone up to the point that the increase in

convective heat transfer results in a decrease in the system temperature, after which the maximum CO content and maximum wall heat flux decreased with increasing gas flow rate.

2. Oxygen composition of inlet gas: A decrease in the oxygen content of the inlet gas (by dilution with an inert gas) results in a decrease in the maximum system temperature, CO content, and wall heat flux but increases the length of the oxidation zone.

3. Oxidation ash build-up: Presence of oxidation ash has the same effect on operating results as a decrease in the inlet gas oxygen content.

Use of either a tubular 5-in.-diam reactor or a 2-1/2-in. slab reactor (approximated by a 2-1/2-in.-diam reactor) was predicted to be feasible by the mathematical model of the reaction system. The oxidation cycle for the 2-1/2-in. slab reactor was estimated to be 3-1/2 hr, while that of the 5-in.-diam reactor was 4 hr (exclusive of reactor heatup and cooldown). Since these cycle times are relatively close together, other factors such as capacity, ease of fabrication, etc., should be the deciding factor for choice of which type of production-scale reactor to use.

11.2 Recommendations

The results of this mathematical analysis of the fixed-bed, graphite-fuel oxidation system have shown several potential problems which should be investigated by additional experimental work. For example, more differential fuel element tests at a variety of operating conditions would allow a better determination of some of the rate constants used in the mathematical analysis of the system. Adequate records of system temperature and other experimental data during oxidation tests in large, fixed beds of the

graphite-fuel would allow a better determination of heat transfer mechanisms and coefficients. Also, actual experimental demonstration of the oxidation cycles which were predicted by the mathematical model would be desirable. If graphite-uranium fuels with properties different from Kiwi-B-1B fuels are to be investigated, then a similar mathematical analysis of the system would also be a useful tool.

12. REFERENCES

1. C. D. Scott, L. E. McNeese, and J. C. Suddath, Processing of Graphite Fuels for Uranium Recovery by Oxidation and Fluorination, ORNL-TM-185 (1962).
2. C. D. Scott, Feasibility of the Oxidation of Graphite-Uranium Fuels with Oxygen. Preliminary Results, ORNL-CF-62-2-35 (1963) (Confidential).
3. L. E. McNeese and C. D. Scott, Recovery of Uranium from Graphite Fuels by Oxidation and Fluorination. I. Design and Initial Operation of an Engineering-Scale Facility, ORNL-3434 (in press) (Confidential).
4. J. W. Prados, Estimation of Reaction and Heat Release Rates of Graphite Oxidation, ORNL-CF-60-10-131 (1960).
5. F. K. Earp and M. W. Hill, "Oxidation of Carbon and Graphite," Industrial Carbon and Graphite, Society of Chemical Industry, London, 1958.
6. R. E. Dahl, Preliminary Evaluation of Chlorine for Use as a Gas Cooled Reactor Safeguard, HW-63902 (1960).
7. L. M. Currie, V. C. Hamister, and H. G. MacPherson, "The Production and Properties of Graphite for Reactors," International Conference on the Peaceful Uses of Atomic Energy, Vol 8, 451-473 (1955).

8. M. Hobson and G. Thodos, "Mass Transfer. Laminar Flow of Gases Through Granular Beds," Chem. Eng. Progr. 47, 370 (1951).

9. C. D. Scott, Kinetics of the Catalyzed Oxidation of Hydrogen, Carbon Monoxide and Methane by Oxygen in a Flowing Stream of Helium, ORNL-3043 (1961).

10. C. D. Scott, Evaluation of the EGCR Catalytic Oxidizer for Oxidation of Hydrogen, Carbon Monoxide, and Methane, ORNL-TM-61 (1961).

11. K. K. Kelly, "Contributions to the Data of Theoretical Metallurgy," Bureau of Mines Bulletin 584 (1960).

12. C. N. Satterfield and H. Resnick, "Simultaneous Heat and Mass Transfer in a Diffusion Controlled Chemical Reaction. Part II. Studies in a Packed Bed," Chem. Eng. Progr. 50, 504 (1954).

13. T. J. Hanrattry, "Nature of Wall Heat Transfer Coefficient in Packed Bed," Chem. Eng. Sci. 3, 209-214 (1954).

14. I. M. Klotz, "The Adsorption Wave," Chem. Review 39, 241 (1946).

15. J. Crank, The Mathematics of Diffusion, Oxford University Press, London (1956).

16. L. E. McNeese, ORNL, unpublished data, January 3, 1963.

17. R. W. Horton, ORNL, personal communication, January 3, 1963.

18. N. A. Lange, editor, Handbook of Chemistry, 3d ed., Handbook Publishers, Inc., 1939.

19. J. G. Knudsen and D. L. Katz, Fluid Dynamics and Heat Transfer, McGraw-Hill, New York, 1958.

20. J. S. Watson, Heat Transfer from Spent Reactor Fuels During Shipping: A Proposed Method for Predicting Temperature Distribution in Fuel Bundles and Comparison with Experimental Data, ORNL-3439 (in press).

21. R. C. Reid, and J. K. Sherwood, The Properties of Gases and Liquids, McGraw-Hill, New York, 1958.

13. LIST OF SYMBOLS

a effective mass transfer area between fluid and CuO pellets, cm^2/cm^3 of bed

a coefficient in heat capacity equation

A constant of integration

A area, cm^2

A constant in Arrhenius expression

b molar density of equivalent graphite in fuel rod, g-mole/cm^3 of fuel rod

b coefficient in heat capacity equation

B constant of integration

c coefficient in heat capacity equation

C concentration of the reacting fluid in the fluid phase, g-mole/cm^3

C_p gas heat capacity, cal/g-mole·°K

d_p diameter of fuel rod, cm

D molecular diffusivity of O_2, cm^2/sec

E activation energy in Arrhenius expression, cal/g-mole

F volumetric gas flow rate, cm^3/sec

F radiative heat transfer geometry factor

G mass flow rate, g/cm^2·sec

h convective heat transfer coefficient, cal/cm·sec°K

J_D mass transfer factor, $\left(k_g \rho / G\right) N_{Sc}^{2/3}$

K_c CO-O_2 reaction rate constant, cm^2/sec·g-mole

k_g mass transfer coefficient across external gas film, cm/sec

k_1 first-order rate constant, g-moles/(cm^2·sec·atm O_2)

k_T gas thermal conductivity, cal/cm·sec·°C

K radiative heat transfer coefficient for fuel rod, cal/cm·sec·°K

m finite difference bed height increment designation

M average molecular weight of gas

n finite difference time increment designation

N number of fuel rods in vertical array

N_{Pr} Prandtl number, $C_p\mu/k_T$, dimensionless

N_{Re} modified Reynolds number, d_pG/μ, dimensionless

N_{Sc} Schmidt number, $\mu/D\rho$, dimensionless

P total pressure, atm

p, partial pressure, atm

q_{12} net transfer of heat from surface 1 to surface 2 radiative

q heat generated in one fuel rod, cal/sec·cm

r radial distance within cylindrical fuel rod, cm

R rate of reaction of carbon or CO, g-moles/sec·fuel rod-cm of length

R gas constant, cal/g-mole·°K

t time, sec

T temperature, °C or °K

v specific volume of gas, cm^3/g-mole

x mole fraction of gas in mixture, dimensionless

z distance in fixed bed from gas inlet, cm

Greek Letters

α effective internal solid-phase porosity, ratio of effective internal void volume to total pellet volume, dimensionless

α radiative absorptivity of a surface

ϵ radiative emissivity of a surface

μ viscosity of oxygen, g/cm·sec

ρ gas density, g-moles/cm^3

σ Stefan-Boltzmann constant

Subscripts and Superscripts

1,2 components or surfaces 1 and 2

c center rod

C carbon

CO carbon monoxide

CO_2 carbon dioxide

E external surface of pellet

F outside of gas film surrounding pellet

g gas phase

H hypothetical reaction zone

I inert gas

I reaction interface within pellet

i ith component

o outside rod or initial

o overall

O_2 oxygen

r fuel rod

S within pellet

s external surface

w reactor wall

14. APPENDIX

14.1 Graphite Oxidation Rate Control by First-Order Kinetics

The graphite oxidation data of Earp and Hill,[5] Dahl[6] and Currie et al.,[7] as presented by Prados[4] can be used to obtain a first-order rate equation in which the reaction rate of oxygen with graphite can be represented as,

$$R_C = k_1 a C_{O_2} , \tag{14.1}$$

if it is assumed that the only reaction-rate controlling mechanism occurs at the reaction site and the reaction site is only at the external surface.

The experimental data from these workers in the temperature range of 500 to 750°C was used to obtain the rate constant k_1, and it was correlated in an Arrhenius-type expression (Table 14.1):

$$k_1 = Ae^{-E/RT} . \tag{14.2}$$

A plot of the experimentally determined k_1, as the logarithm of k_1, vs reciprocal time 1/T, gave a reasonably straight line (Fig. 14.1) which was then used to obtain the constants, A and E, for Eq. 14.2. The value of A was determined to be 2×10^4 from the intercept of the curve with the k_1 axis at 1/T = 0. The slope of the log k_1-vs-1/T-plot was used to obtain the value of the activation energy E. The slope was found to be -21,400. This must equal to -E/R; however, since R ≈ 2.0 cal g-mole^{-1} °K^{-1}, then

$$E = 2 \times 21{,}400 = 42{,}800 \text{ cal/g-mole} .$$

14.2 Physical Properties of Gases

Where the heat capacity and thermal conductivity of the gas phase were needed, these properties of the gas mixture were approximated by a

Table 14.1. Graphite Oxidation Rates from the Data Presented by Prados[4]

Temp. (°C)	Observed Rate $\frac{\text{g-moles}}{(\text{g-moles total})(\text{hr})(\text{atm } O_2)}$	Shape of Sample and Dimensions	External Surface* cm^2 per g-mole	Rate $\left(\frac{\text{g-mole}}{cm^2 \cdot \text{sec} \cdot \text{atm } O_2}\right)$	Source
500	1.15×10^{-3}	Rectangular block,	32.2	1.05×10^{-8}	Earp and Hill[5]
550	5.25×10^{-3}	3.4 cm x 0.9 cm x 0.95 cm	32.2	5.20×10^{-8}	Earp and Hill[5]
600	3.45×10^{-2}	3.4 cm x 0.9 cm x 0.95 cm	32.2	3.12×10^{-7}	Earp and Hill[5]
650	1.22×10^{-1}	3.4 cm x 0.9 cm x 0.95 cm	32.2	1.10×10^{-6}	Earp and Hill[5]
700	3.32×10^{-1}	3.4 cm x 0.9 cm x 0.95 cm	32.2	3.11×10^{-6}	Earp and Hill[5]
550	1.81×10^{-2}	Hollow cylinders,	66.2	7.95×10^{-8}	Dahl[6]
600	5.67×10^{-2}	0.426-in. OD x 2 in. long	66.2	2.50×10^{-7}	Dahl[6]
700	6.39×10^{-1}	0.25-in. ID x 2 in. long	66.2	2.80×10^{-6}	Dahl[6]
750	1.81	0.25-in. ID x 2 in. long	66.2	7.95×10^{-6}	Dahl[6]
600	1.41×10^{-2}	Solid cylinder,	11.25	3.64×10^{-7}	Currie *et al.*[7]
700	1.58×10^{-1}	1.25-in. OD x 2 in. long	11.25	4.10×10^{-7}	Currie *et al.*[7]

*Graphite density assumed to be 0.143 g-moles/cc

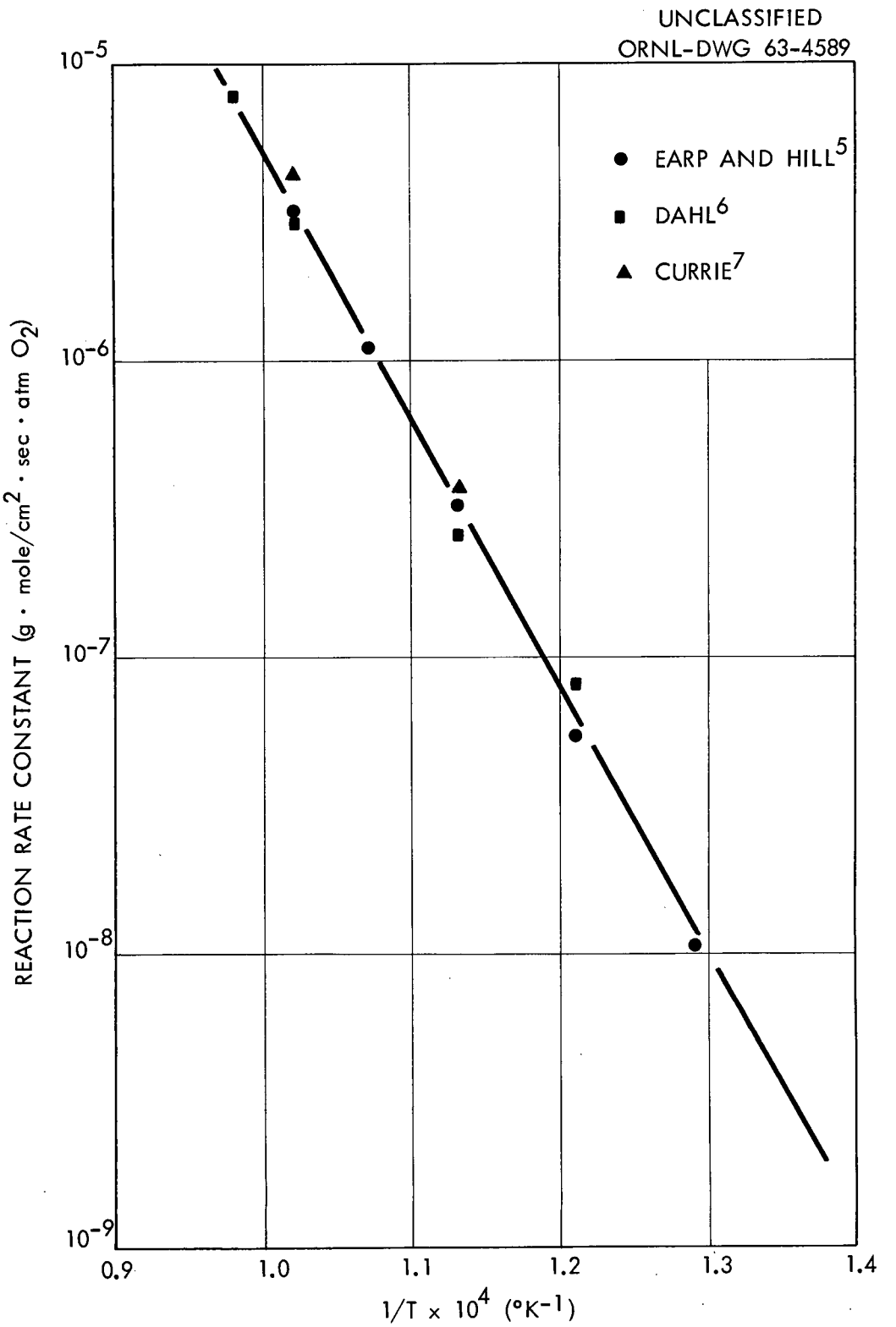

Fig. 14.1. Arrhenius Plot of Reaction Rate Constant for the Graphite-Oxygen Reaction from Data Presented by Prados.[4]

linear combination of the individual components. The individual gas heat capacity and thermal conductivity properties must be correlated as functions of temperature. These correlations were obtained either from the literature or derived from literature data.

14.2.1 Thermal Conductivity

The thermal conductivity of the individual gases were obtained from literature sources.[18,19] These values can be correlated as a function of temperature by a simple linear relationship:

$$k_{T_i} = A_i T_g + B_i \ , \tag{14.3}$$

where

A_i and B_i are constants for the ith component .

Thermal conductivities for oxygen, nitrogen and CO are reasonably close together; therefore, they were grouped together, and a single correlation was used. The equations as determined from a plot of data (Fig. 14.2) which represent the thermal conductivity correlations in the temperature range of 200-800°K are:

for oxygen, nitrogen, or CO,

$$k_{T_{O_2}} = 1 \times 10^{-5} + 1.6 \times 10^{-7} T_g \ , \tag{14.4}$$

for CO_2,

$$k_{T_{CO_2}} = 1.4 \times 10^{-5} + 1.8 \times 10^{-7} T_g \ . \tag{14.5}$$

14.2.2 Heat Capacity

Heat capacity data can be presented as a function of temperature in the following type of expression:

$$C_{P_i} = a_i + b_i T_g + c_i T_g^{-2} \ . \tag{14.6}$$

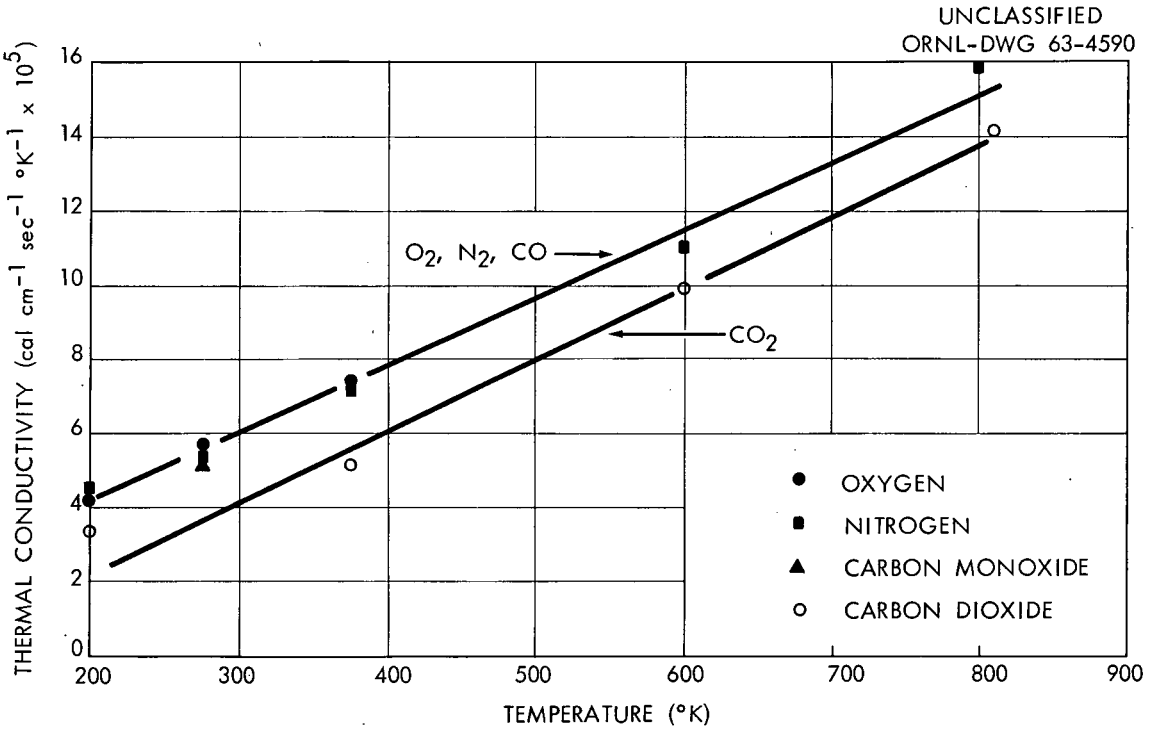

Fig. 14.2. Thermal Conductivity of O_2, N_2, CO, and CO_2 as a Function of Temperature. From references 18 and 19.

Correlations for oxygen, nitrogen, CO, and CO_2 were obtained from a Bureau of Mines publication on the subject[11] (Table 14.2):

Table 14.2. Heat Capacity Data for Oxygen, Nitrogen, CO, and CO_2[11]

Component	a	C_p	
		$b \times 10^3$	$C \times 10^{-5}$
O_2	7.16	1.0	-0.4
N_2	6.83	0.9	-0.12
CO	6.79	0.98	-0.11
CO_2	10.57	2.10	-2.06

The heat capacity of oxygen, nitrogen, and CO are reasonably close, therefore, a common heat capacity correlation was used for these components:

$$C_p = 7.2 + 0.00086T \ . \tag{14.7}$$

14.3 Radiative Heat Transfer Constants

The radiative heat transfer that will occur between one fuel rod and other fuel rods and the reactor wall can be expressed by:

$$q_{12} = \sigma AF(T_1^4 \epsilon - T_2^4 \alpha) \ , \tag{14.8}$$

where q_{12} is the rate of net heat transfer from surface 1 to 2. If the emissivity ϵ and absorptivity α are approximated to be 1.0, and if σ, A, and F are combined into one term:

$$q_{12} = K_{12} \ (T_1^4 - T_2^4) \ . \tag{14.9}$$

In this study two such expressions are used:

Heat transfer from center rod,

$$q_c = K_c \ (T_c^4 - T_o^4) \ , \tag{14.10}$$

and heat transfer from outside rods,

$$q_o = K_o(T_o^4 - T_w^4) \quad . \tag{14.11}$$

When the fuel rods are arrayed loosely so that each fuel rod can "see" all other rods and a large portion of the wall, the shape or view factor F_{12} must be determined. J. S. Watson[20] has correlated a large number of these view factors as a function of rod size and type of array (square array, etc.).

When the fuel rod array is tightly packed, as will be the case for a production reactor, a much simpler method for determination of the radiative heat transfer coefficient may be used. For example, consider the 5-in.-diam reactor in which 29 fuel rods are to be placed. One possible type of fuel-rod array is a single rod in the center surrounded by two concentric rows of rods containing 11 and 17 rods, respectively (see Fig. 14.3).

Net heat transfer by radiation from the center rod to the middle row of rods can be expressed by:

$$q_c = q = \sigma A(T_c^4 - T_m^4) \quad , \tag{14.12}$$

where

A = area of one rod,

T_m = temperature of middle row of rods.

Net heat transfer from the middle row of rods to the outside rod (assuming equal heat generation per rod and only half of rod area which can "see" outside rods) can be expressed by:

$$q_m = 12\ q = \sigma(11A/2)(T_m^4 - T_o^4) \quad . \tag{14.13}$$

Finally, the heat transfer from the outside rods to the wall can be expressed by:

[redacted]

ORNL-DWG 63-4591

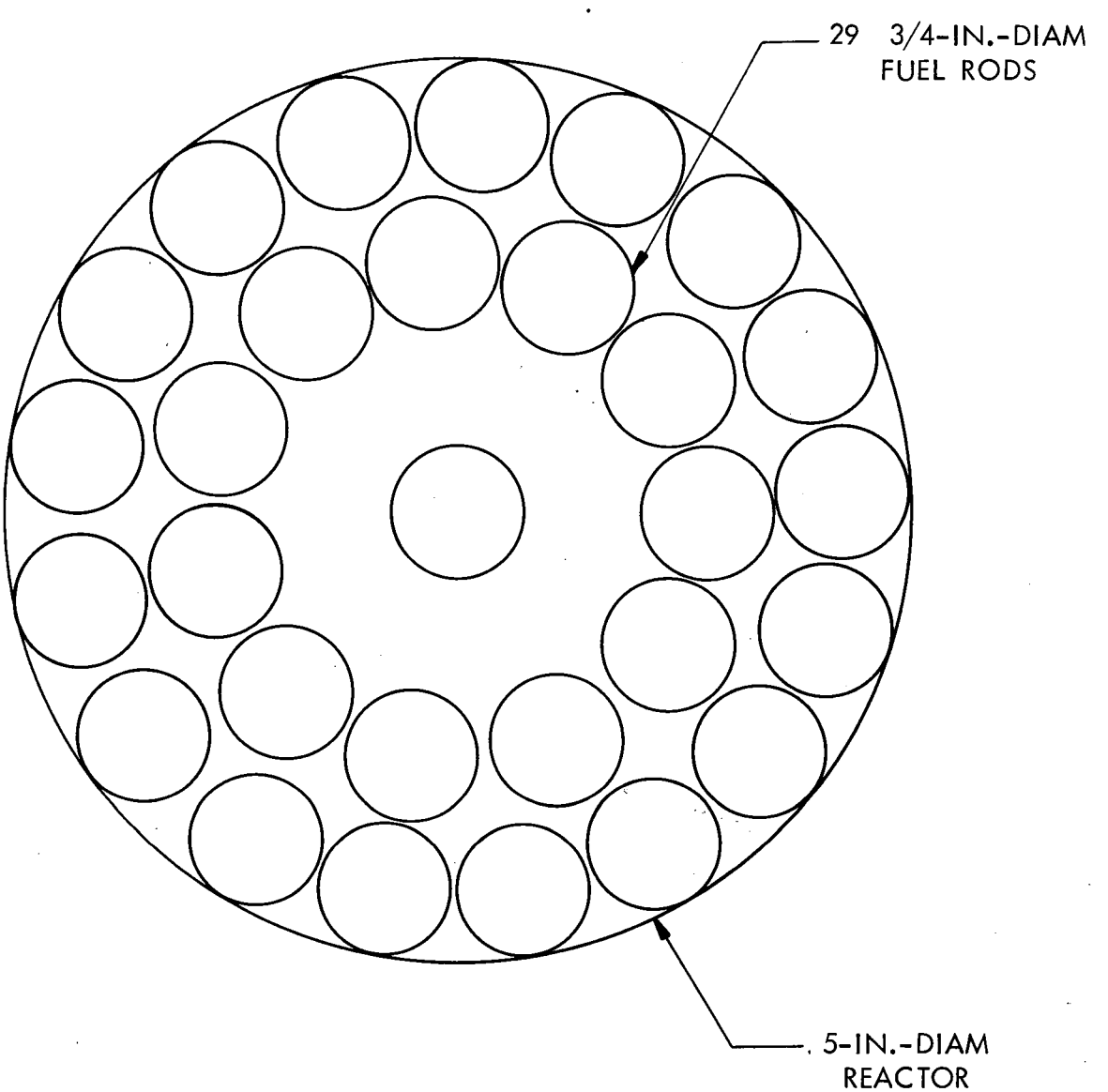

Fig. 14.3. Section of Assumed Array of 29 3/4-in.-diam Fuel Rods in a 5-in.-diam Reactor.

$$q_o = 29\ q = \sigma(17A/2)(T_o^4 - T_w^4) \quad . \tag{14.14}$$

Equation (14.14) is in the form of Eq. (14.11), where

$$K_o = \sigma(17A/2) \quad . \tag{14.15}$$

Combining Eqs. (14.12) and (14.13) one obtains:

$$q_c = \frac{\sigma A}{1 + \frac{24}{11}} (T_c^4 - T_o^4) \quad . \tag{14.16}$$

Therefore, the radiative heat transfer coefficient for the center rod is:

$$K_c = \frac{\sigma A}{1 + \frac{24}{11}} \quad . \tag{14.17}$$

14.4 Differential Fuel Section Test

One differential element test was made in which a section of a fuel rod (full diameter but short height) was exposed to oxygen at 900°C. The fuel-rod section was suspended from one side of the balance arm of an analytical balance (Fig. 8.1) into a heated quartz tube. Oxygen was passed up the tube where it was preheated prior to contacting the fuel-rod element. The effluent from the device was periodically sampled by a gas adsorption chromatograph for its oxygen, CO, and CO_2 content, and the weight change of the fuel-rod section was recorded every 15 sec.

The reaction rate of graphite with oxygen as weight loss of carbon per unit time (with corrections for metal carbide oxidation) as a function of time (Fig. 14.4) was determined for the one differential section test. The CO reaction rate was determined from the graphite reaction rate and the amount of CO and CO_2 in the off-gas. This data was used to determine some of the reaction rate constants.

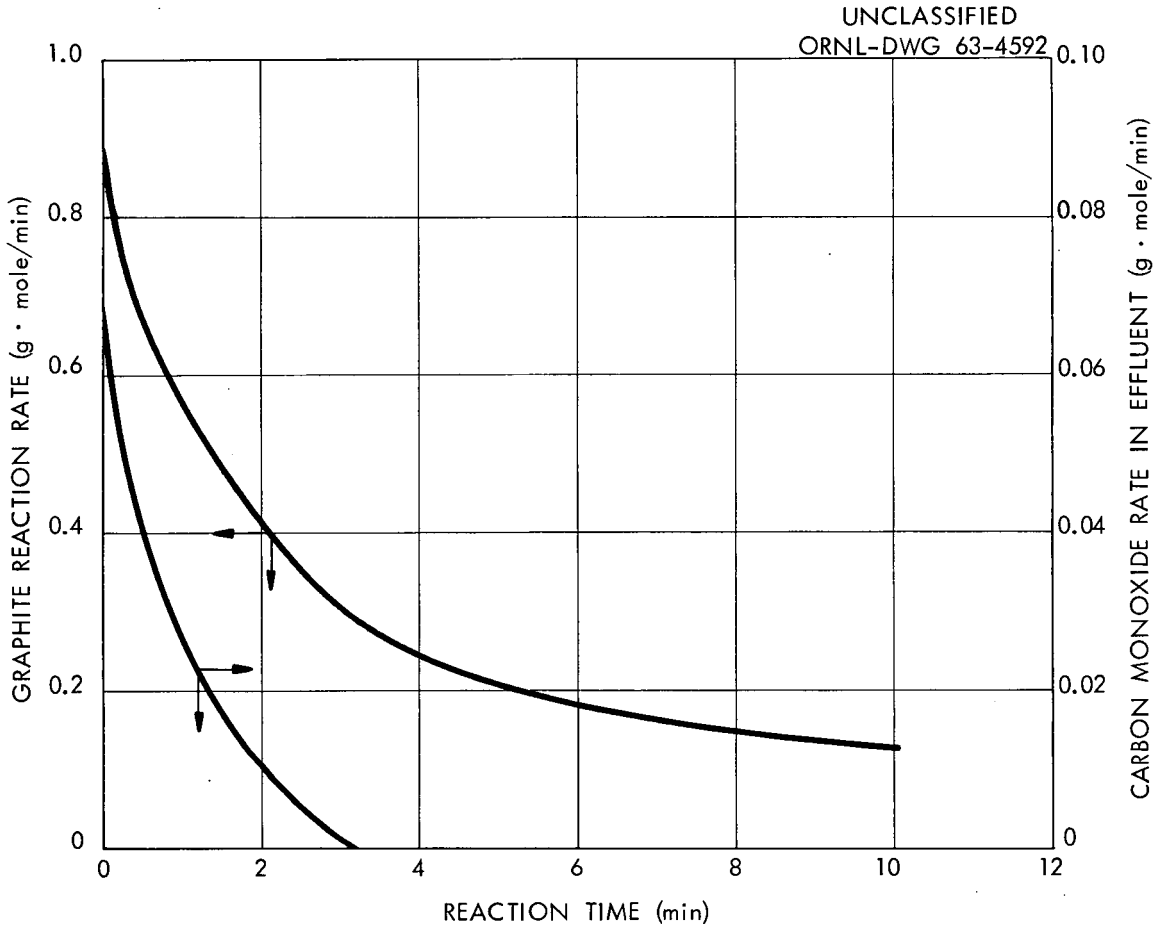

Fig. 14.4. Reaction Rates for Differential Fuel Rod Section Test Made at 900°C.

14.4.1 Rate Constants for CO Oxidation

The rate constants for CO oxidation can be determined from Eqs. (8.4) and (8.5). At the beginning of reaction the rate constant k_{c_1} can be determined from:

$$k_{c_1} = \frac{R_{CO}}{(C_{O_2})^2} . \qquad (14.1)$$

The reaction rate of CO to oxygen at the beginning of the test was:

$$R_{CO} = 0.000879 \text{ g-moles cm}^{-1} \text{ sec}^{-1} \text{ rod}^{-1} ;$$

and the oxygen concentration was::

$$C_{O_2} = 1.13 \times 10^{-5} \text{ g-moles/cc} .$$

Then the rate constant is:

$$k_{C_1} = \frac{8.79 \times 10^{-4}}{1.28 \times 10^{-10}} = 6.85 \times 10^{6} \text{ cm}^2/\text{sec} .$$

After the reaction had progressed for 2 min, the CO reaction rate was:

$$R_{CO} = 0.000893 \text{ g-mole cm}^{-1} \text{ sec}^{-1} .$$

Use of Eq. (8.5) then results in:

$$k_{c_2} = \frac{\dfrac{0.000893}{1.28 \times 10^{-10}} - 6.85 \times 10^{6}}{(0.860 - 0.602} = 5.05 \times 10^{5} \text{ sec}^{-1} .$$

14.4.2 Internal Mass Transport Property

The internal mass transport property αD can be determined from the carbon reaction rate after the reaction has occurred sufficiently long to allow appreciable ash buildup. Equation (8.6) can be used to determine αD:

$$\alpha D = \frac{R_C \ln \frac{r_E}{r_I}}{4\pi C_{O_2}} . \qquad (14.18)$$

At t = 10 min, the carbon reaction rate was: $R_C = 0.0002$ g-mole cm^{-1} sec^{-1} ; and the position of the reaction interface was: $r_I = 0.830$ cm. Equation (14.18) then gives:

$$\alpha D = \frac{0.00022 \ln \frac{0.950}{0.830}}{(4\pi)(1.13 \times 10^{-5})} = 0.217 \text{ cm}^2/\text{sec} .$$

The molecular diffusivity D can be determined to be 2.56 cm^2/sec for oxygen at the conditions of the test;[21] therefore, the effective porosity α will be 0.085.

ORNL-3456
C-44b — Nuclear Technology — Chemistry and Chemical Engineering
M-3679 (31st ed.)

INTERNAL DISTRIBUTION

1-3. Central Research Library
4-5. ORNL — Y-12 Technical Library Document Reference Section
6-15. Laboratory Records Department
16. Laboratory Records, ORNL R.C.
17. R. E. Blanco
18. J. C. Bresee
19. R. E. Brooksbank
20. K. B. Brown
21. W. H. Carr
22. W. L. Carter
23. G. I. Cathers
24. F. L. Culler
25. D. E. Ferguson
26. L. M. Ferris
27. B. C. Finney
28. T. A. Gens
29. H. W. Godbee
30. H. E. Goeller
31. B. A. Hannaford
32. R. W. Horton
33. F. G. Kitts
34. C. E. Lamb
35. C. E. Larson
36. W. D. Manly
37. G. B. Marrow (Y-12)
38. L. E. McNeese
39. R. P. Milford
40. E. L. Nicholson
41. L. G. Overholser
42. A. D. Ryon
43. W. F. Schaffer
44. C. D. Scott
45. M. J. Skinner
46. S. H. Smiley
47. A. E. Spaller
48. J. C. Suddath
49. J. A. Swartout
50. J. W. Ullmann
51. C. D. Watson
52. A. M. Weinberg
53. M. E. Whatley
54. H. B. Whetsel
55. R. G. Wymer
56. P. H. Emmett (consultant)
57. J. J. Katz (consultant)
58. T. H. Pigford (consultant)
59. C. E. Winters (consultant)

EXTERNAL DISTRIBUTION

60. E. L. Anderson, Jr., Atomic Energy Commission, Washington
61. R. D. Baker, Los Alamos Scientific Laboratory
62. L. C. Corrington, SNPO
63. D. C. Davis, Oak Ridge Operations Office
64. L. P. Hatch, Brookhaven National Laboratory
65. J. A. McBride, Idaho Chemical Processing Plant
66. W. S. Scheib, Atomic Energy Commission, Washington
67. J. L. Schwennesen, Atomic Energy Commission, Washington
68. G. Strickland, Brookhaven National Laboratory
69. Research and Development Division, AEC, ORO
70-271. Given distribution as shown in M-3679 (31st ed.) under Nuclear Technology — Chemistry and Chemical Engineering category